AC-DRL TR69-12
MAY 1970

GENERAL MOTORS CORPORATION

SAMSO REPORT NO. TR70-186

CALIBRATION AND USE OF SPHERICAL AND CYLINDRICAL ELECTROSTATIC PROBES FOR HYPERSONIC WAKE STUDIES

I.P. French, R.A.Hayami, T.E. Arnold, M. Steinberg
and
J.P. Appleton and A.A. Sonin
of the
MECHANICAL ENGINEERING DEPARTMENT,
MASSACHUSETTS INSTITUTE OF TECHNOLOGY

Sponsored by
ADVANCED RESEARCH PROJECTS AGENCY
(ARPA Order No. 1341)
and
SPACE AND MISSILE SYSTEMS ORGANIZATION
AIR FORCE SYSTEMS COMMAND
under
Contract No. FO4701-69-C-0125
(Effective 10 October 1968)

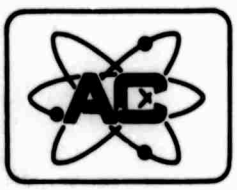

Aerospace Operations Department

AC ELECTRONICS - DEFENSE RESEARCH LABORATORIES

SANTA BARBARA, CALIFORNIA

H6

DISPOSITION INSTRUCTIONS

Destroy this report when it is no longer needed. Do not return it to the originator.

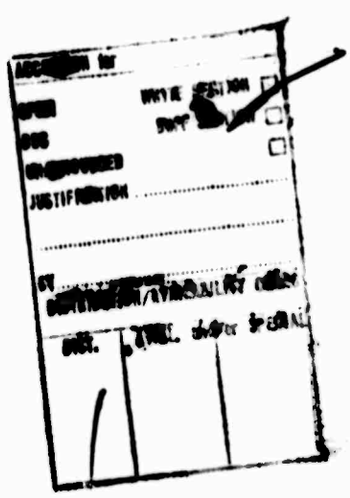

COPY NO. 54

AC-DRL TR69-12
MAY 1970

GENERAL MOTORS CORPORATION

SAMSO REPORT NO. TR70-186

CALIBRATION AND USE OF SPHERICAL AND CYLINDRICAL ELECTROSTATIC PROBES FOR HYPERSONIC WAKE STUDIES

I.P. French, R.A.Hayami, T.E. Arnold, M. Steinberg
and
J.P. Appleton and A.A. Sonin
of the
MECHANICAL ENGINEERING DEPARTMENT,
MASSACHUSETTS INSTITUTE OF TECHNOLOGY

Sponsored by
ADVANCED RESEARCH PROJECTS AGENCY
(ARPA Order No. 1341)
and
SPACE AND MISSILE SYSTEMS ORGANIZATION
AIR FORCE SYSTEMS COMMAND
under
Contract No. FO4701-69-C-0125
(Effective 10 October 1968)

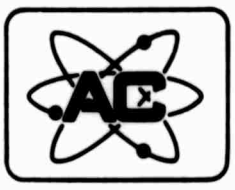

Aerospace Operations Department

AC ELECTRONICS - DEFENSE RESEARCH LABORATORIES

SANTA BARBARA, CALIFORNIA

FOREWORD

The research work reported herein was jointly supported by the Advanced Research Projects Agency (ARPA) of the Department of Defense and the Space and Missile Systems Organization (SAMSO), Air Force Systems Command, under Contract No. F04701-69-C-0125. The contract monitor for this work is Capt. L. Hillebrand (SMYSE) at Norton Air Force Base, California 92409. The work was performed at AC Electronics - Defense Research Laboratories (AC-DRL) of General Motors Corporation in Santa Barbara, California.

Some of the material in this report was originally prepared for presentation at the 1969 IEEE (3rd) International Congress on Instrumentation in Aerospace Simulation Facilities, held at the Polytechnic Institute of Brooklyn Graduate Center on 5—8 May 1969 and subsequently published in the proceedings of that meeting (pages 34—42, ICIASF '69 Record). The present work is a continuation of that previously reported.

The interest of the technical monitors for this work at Aerospace Corporation is appreciated by the authors, who also wish to express their thanks to R. I. Primich of AC-DRL for his valuable advice and encouragement, to J. D. Taylor for the operation of the shock tube, and to F. J. Ramsey for his work on the probes. The authors are also grateful to P. E. Robillard and S. Zivanovic who developed much of the electronics associated with logarithmic amplifiers used to process the electrostatic probe signals. Finally, it is a pleasure to acknowledge valuable discussions with W. E. Sharfman and coworkers at Stanford Research Institute.

This technical report has been reviewed and is approved.

Duane C. Berck
Contracting Officer
Space and Missile Systems
Organization (AFSC)
Norton Air Force Base
California 92409

ABSTRACT

An experimental shock tube program was undertaken in order to calibrate electrostatic probes which may be used to make point ion density measurements in continuum flowing plasmas.

The empirically derived formula which relates the ion density to the measured probe current was obtained in terms of the appropriate similarity parameters and, over the range of conditions covered, was found (for spherical probes) to be expressible in the form:

$$i = (-\emptyset)^{\frac{1}{1+0.61\,\ell n(1+r/\lambda_D)}} [1.2+0.09\,Re]$$

where i is the Nusselt number for mass transfer of the positive ions, $(-\emptyset)$ is a dimensionless probe potential, λ_D/r is the ratio of the Debye length to probe radius, and Re is the flow Reynolds number based on the probe diameter. This empirical correlation was used to interpret the ion currents collected by a radial array of negatively biased spherical probes which were positioned so as to intercept the ionized wake of a hypervelocity model in a ballistics range. The integrated ion densities were found to be in good accord with the integrated electron densities which were simultaneously measured using microwave methods. The application of the electrostatic probe measuring technique to the study of negative-ion chemistry in wakes is also illustrated and briefly discussed.

CONTENTS

ILLUSTRATIONS

I. INTRODUCTION

The desirability of being able to make point electron density measurements in the turbulent wakes of hypervelocity projectiles has long been recognized as a necessary step toward gaining a proper understanding of their structure and their radar scattering characteristics. Although ballistics ranges do provide an appropriate laboratory environment for making such measurements and, indeed, measurements of average electron densities as a function of distance behind the projectile have been obtained,[1, 2] no reliable point measurements of electron density fluctuations have so far been made.

In a recent paper, Sutton[3] proposed a ballistics range experiment which might allow such measurements to be performed with cylindrical collision-free Langmuir probes, held in tension so as to avoid the problem of probe bending. In order to operate the probe in the collision-free regime and at the same time have a turbulent wake, relatively large ballistic models and low environmental pressures are required. (Sutton's calculations were based on the theoretically computed wake conditions behind a 6.8 cm-diameter sphere traveling at 4.72 km/sec in an ambient pressure of 10 torr.) Unfortunately, the ballistics range experiments carried out to date at AC Electronics - Defense Research Laboratories' (AC-DRL) facility have been conducted with smaller models (typically spheres which range in diameter from 0.5 cm to 2.5 cm) and at pressures greater than 10 torr.

There are a variety of reasons which lead to the choice of a particular set of conditions for operation of a ballistics range. These depend upon the type of measurement that is to be made; however, one of the most important factors which predicates against large-scale models is the fairly obvious economic one that the costs of the ballistics range facility and its operation increase at a greater than linear rate with increasing model size for a typical reentry speed of about 6 km/sec. It seemed reasonable therefore, to examine the possibility of using electrostatic probes which can be operated in the continuum regime, where the mean-free-path is smaller than the characteristic probe size. The obvious advantage to be gained by adopting this approach is that one can continue to use the existing ballistics ranges and their established methods of operation to investigate wake structure over a considerable range of body sizes (over at least a factor of 5 in scale size).

Clearly, the crucial problem in using continuum electrostatic probes in the range environment is the method of interpreting the probe current measurements. Although a number of theoretical treatments of probe response in continuum, flowing plasmas are available (e. g., Lam,[4] Hoult,[5] Sonin,[6] and Su,[7] to mention only a few representative works), the complexity of the situation is such that each analysis is addressed to specific limiting conditions of flow, probe geometry, etc., and a unified theory spanning the wide range of conditions encountered in a ballistics range is not at present available. Consider, for example, a probe about one millimeter in diameter under typical range conditions.[2] Except in the very near wake (less than about a hundred body diameters downstream of the projectile) the flow in the wake is subsonic,[8] and the primary parameters governing the probe response are expected to be the local Reynolds number based on probe diameter, Re, the ratio of Debye length to probe radius, λ_D/r, and the dimensionless probe potential, $\phi = eV/kT$. As the probe passes from the near wake to the far wake, the Reynolds number ranges from about 200 to 4, and the Debye length ratio from about 10^{-2} to 1, as illustrated in Figure 1. The available theories, on the other hand, are tailored largely for the limiting conditions of either very small or very large Debye lengths and very small or large Reynolds numbers, as indicated in the figure (note that the situation in Figure 1 is somewhat oversimplified, since the third coordinate of the similarity parameter space, the probe potential eV/kT, has been omitted). Another deficiency in the available theories is their inability to deal with ion collection by the downstream side of the probe, where flow separation occurs; thus in a turbulent wake it is generally impracticable to use probes with collecting surfaces always oriented into the flow.

It is apparent, therefore, that an experimental calibration of probes is required in flow conditions simulating those of the ballistics range. Such a calibration, and its application in an investigation of hypersonic wakes, is presented in this report. The probe calibration experiments were carried out using a shock tube where the variation of the electron density behind the primary shock could be measured using a focused microwave interferometer.[2, 9] Most experiments reported here were done with spherical probes so as to eliminate the influence of flow direction on probe response, and only ion collection at negative probe potentials was considered. The range of the probe Reynolds number and the ratio of the Debye length to probe radius covered in this calibration is also illustrated in Figure 1.

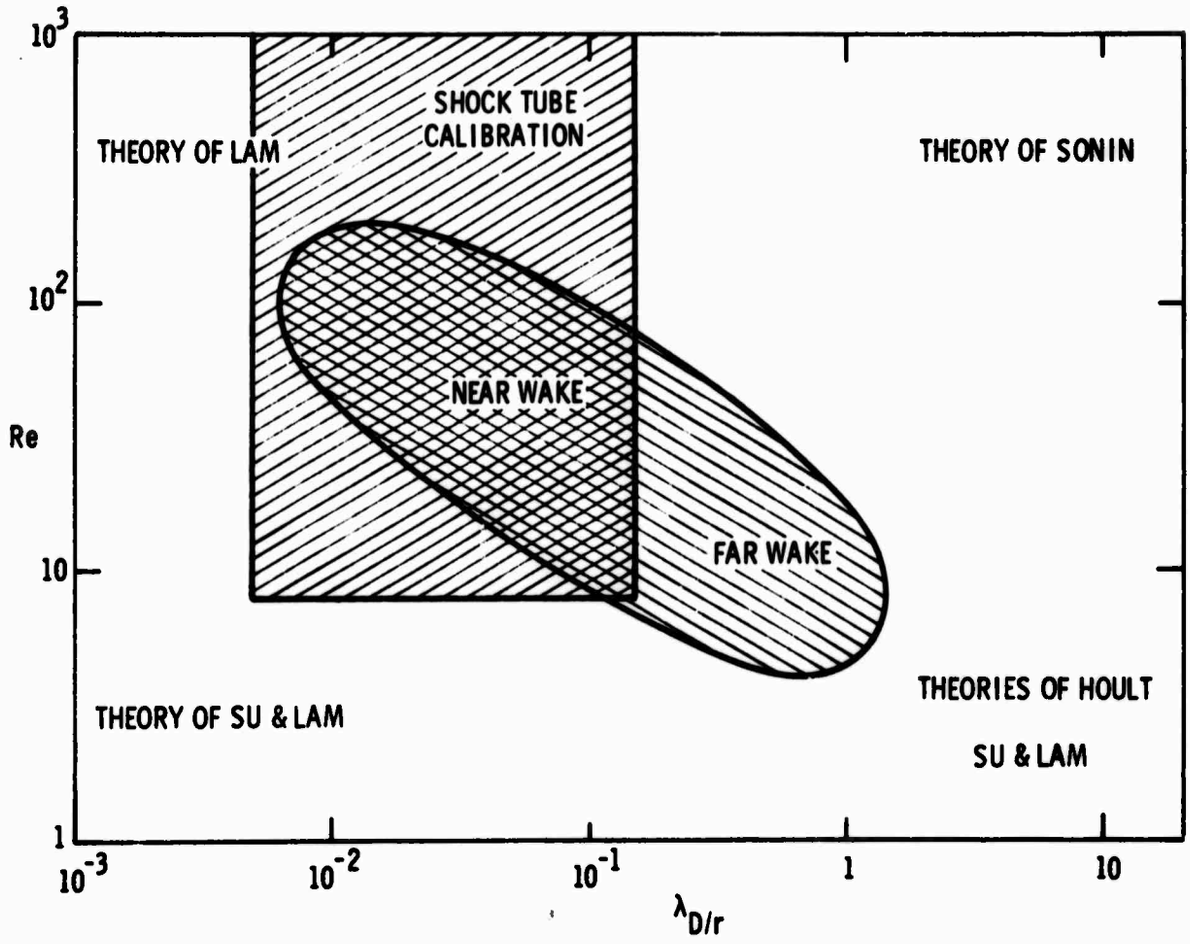

Figure 1 Range of Probe Re and λ_D/r Covered in a Typical Wake and also in the Present Calibration. Also shown are limits of available theories.

The spherical probe calibration part of the experiments described here is discussed in Section II (see Appendix A for cylindrical probe calibration) and its application to measuring mean ion density profiles in the wakes of hypervelocity projectiles is demonstrated in Section III. Although such probes are also capable of providing quantitative information on the fluctuating components of the ion density, this report is limited to a discussion of the mean density profiles.

II. THE SHOCK TUBE CALIBRATION

A. EXPERIMENTAL APPARATUS

A pressure-driven stainless-steel shock tube having an internal diameter of 15 cm was chosen as a means of providing a flowing plasma whose temperature, pressure, and flow velocity in the region behind the primary shock could be accurately calculated from the known initial conditions and measured shock velocity. Details of construction and the method of operation of the shock tube have been described elsewhere in the literature[10] and will not be repeated here.

The test gas used was argon, to which small amounts of acetylene and oxygen (1% C_2H_2 and 5% O_2) were added to produce measureable ionization levels behind the shocks at relatively low temperatures by the process of chemi-ionization. The pressure behind the shock (p_2) was varied between 5 and 1200 torr. In these calibration experiments it was not necessary that the precise reaction kinetics of the chemi-ionization process should be known, since the temporal variation of the electron density was measured directly, using a microwave interferometer (see below). However, it is generally believed that the dominant positive ion which persists after the initial reaction zone in lean acetylene flame[11, 12] and shock-tube studies[10, 13] is H_3O^+, which is then removed via a dissociative recombination reaction of the type:

$$H_3O^+ + e^- \rightarrow H_2O + H \text{ (or other neutral products)} \qquad (1)$$

Since it was necessary to have some reasonably reliable estimate of the diffusion coefficients of the charged species for the method of data reduction used, H_3O^+ was assumed to be the dominant positive ion in the plasma decay region behind the shock wave. (Even if other ions such as CHO^+ made significant contributions to the total positive ion density, it is believed that this would not constitute a significant error since it would enter only through the diffusion coefficient, which is inversely proportional to the square root of the mass.) The only negatively charged species present were electrons, since the temperature range of the present experiments (2000°–7000°K) was too high to allow any significant concentration of molecular negative ions such as O^- and O_2^- to be formed.

The experimental arrangement in the test section of the shock tube is illustrated in Figure 2. The passage of the primary shock wave through the test gas produced a region of extremely rapid ionization which was followed by a region of much slower decay. Within these regions the electron density was measured with a focused microwave probe,[2, 9] and the ion density was monitored with spherical ion probes.

The 70GHz focused-beam microwave interferometer used to make the electron density measurements in the shock tube operates on essentially the same principles as reported previously.[9, 14] The main virtues of this system are that, through the use of focusing, high spatial and temporal resolution is achieved in the plasma-interaction region. Also, through appropriate design there is essentially free-space propagation of plane waves in the focal region,[15, 16] permitting very straightforward interpretation of the measured quantities.

A schematic view of the microwave module is shown as part of Figure 2. Dielectric lenses are used to focus the microwave energy into the flow-through section which samples the near-axis flow in the shock tube. An f/2 lens was chosen to give a depth of field greater than the width of the flow-through section (6.4 cm vs 3.8 cm).

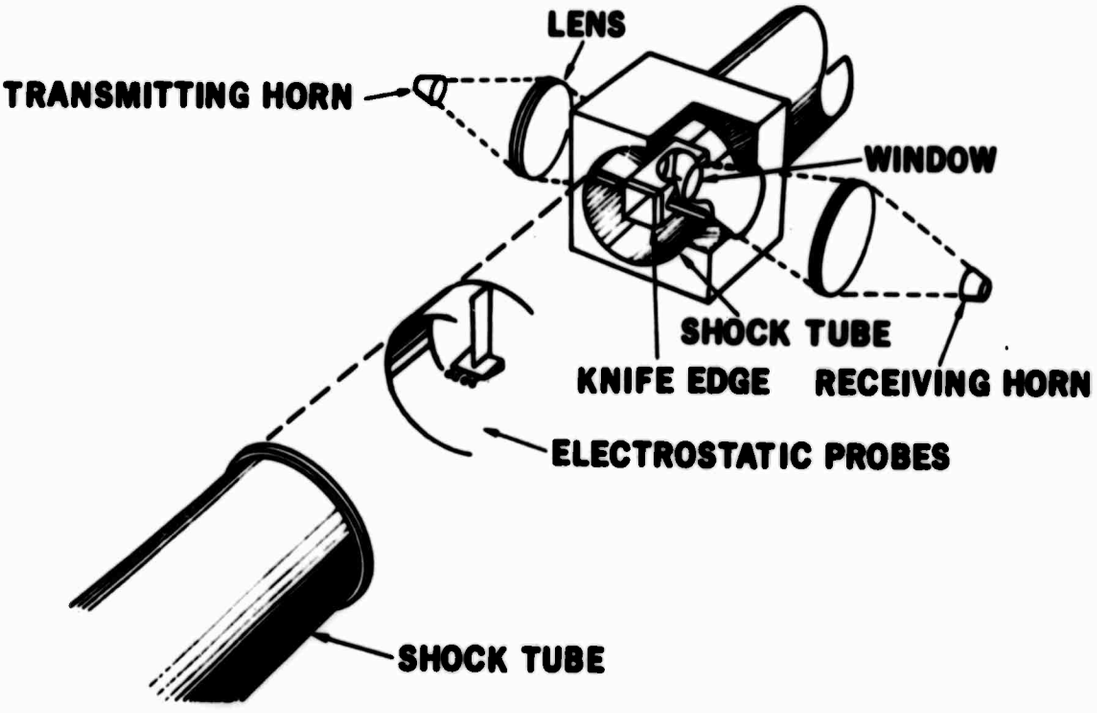

Figure 2 Electrostatic Probes and Focused Microwave Interferometer in Shock Tube

Measurements with irises lined with microwave absorber showed that 90% of the energy was confined in a cylinder 1.6 cm in diameter. Flush dielectric windows are inset in the sides of this section to permit transmission of the focused beam through the ionized flow. The thickness of the windows was machined to an integral number of half-wavelengths to eliminate multiple reflections of the microwave energy. The measured standing-wave ratio in the box was less than 1.005. The diameter of the windows (3.8 cm) was sufficiently larger than the focused-beam diameter so that there were negligible effects on the transmission properties of the focused beam.

The receiver circuitry used autodyne mixing with enough bias for the mixer provided by the reference path that the output is $A(t) \sin \theta(t)$, where $A(t)$ and $\theta(t)$ are the time-varying amplitude and the phase change of the signal transmitted through the ionized flow. Through the use of an additional receiver circuit, $A(t) \cos \theta(t)$ is also recorded, permitting $A(t)$ and $\theta(t)$ to be derived explicitly. These quantities are then converted to collision frequency and electron density. The dynamic range of this instrument is about 10^{10} to 10^{13} cm^{-3}; the electron densities in the tests were in the range of 10^{10} to 3×10^{11} cm^{-3} and the plasma was therefore always very underdense. The largest value of electron collision frequency measured (for $p_2 \approx 1000$ torr and $Re \approx 2000$ to 8000) was 2×10^{11} sec^{-1}. This is still well below the operating frequency (4.4×10^{11} radians sec^{-1}). Since the measured attenuation was always below 5%, the phase change is almost directly proportional to the electron density.[17] Figure 3a shows a typical oscilloscope display of the $A(t) \sin \theta(t)$ signal measured behind an incident shock.

The spherical ion probes (diameters 0.76 mm and 3.2 mm) were mounted on an insulated sting (0.5 mm in diameter) which protruded about one probe diameter in front of the leading edge of a thin wedge-shaped support. This probe assembly was positioned a short distance ahead of the microwave box and sufficiently far off the shock-tube axis that no disturbance from it could influence the flow within the box. Nearly all the measurements to be reported were made using this configuration.

The probes were biased at voltages ranging from -1.4 to -30 V relative to the shock-tube ground. A block diagram of the electrostatic probe circuit is shown in Figure 4. The voltage signal generated by the passage of the probe current through the load resistance was passed through an X100 operational amplifier and the resulting voltage signal was displayed on an oscilloscope. This system thus gave both large bandwidth

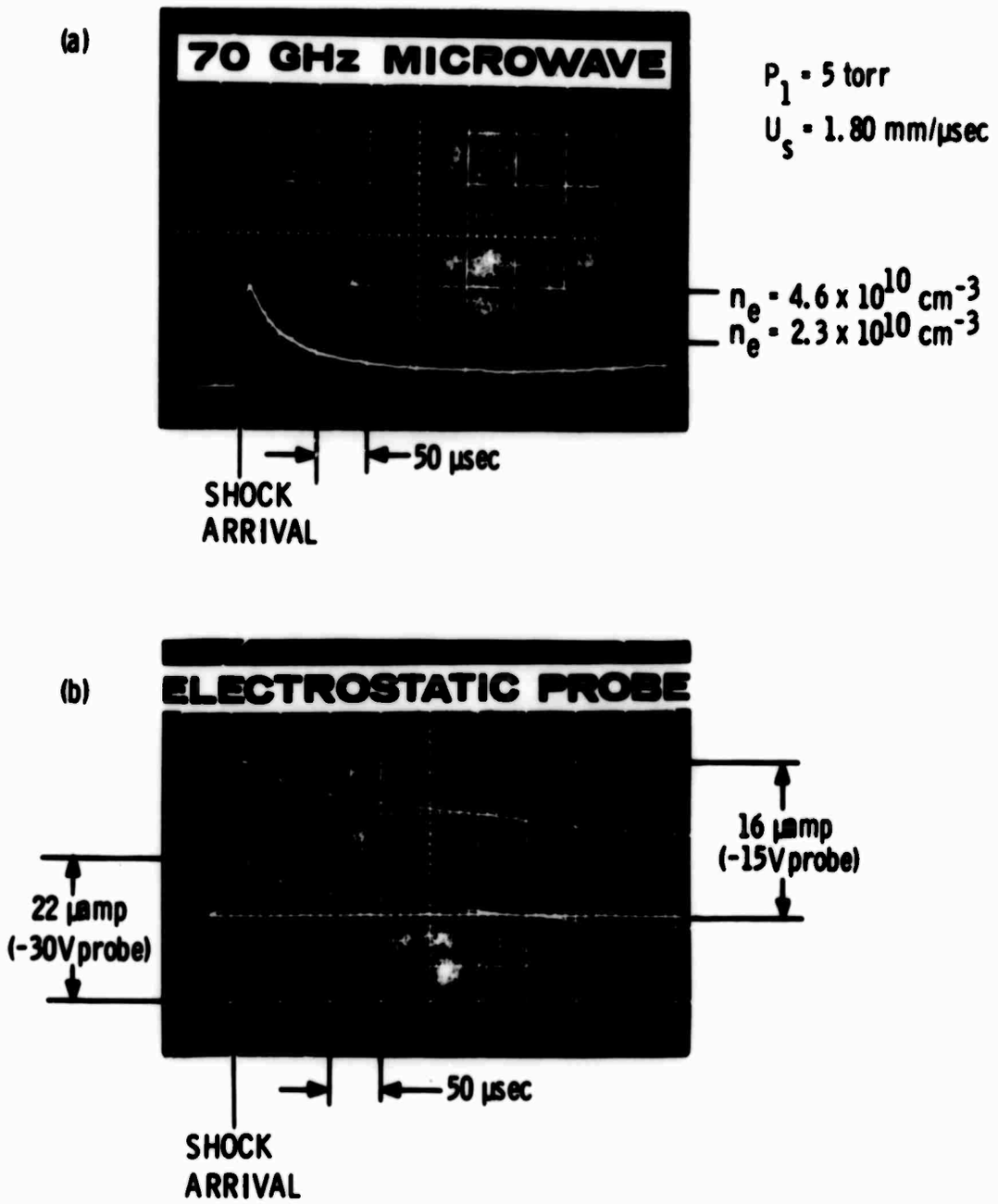

Figure 3 Response of 70GHz Microwave Interferometer A sin ϕ(t) and Electrostatic Probes to Shock-Ionized Acetelyne-Oxygen and Argon Mixture

and dynamic range. Figure 3b shows the measured probe currents, displayed on a logarithmic vertical scale, from two probes biased at -15 V and -30 V; the displays shown in Figures 3a and 3b were obtained behind an incident shock in the same experimental test. One major division on the vertical scale of Figure 3b corresponds to approximately a factor of 10 in probe current.

A few measurements were made behind reflected shocks where the gas velocity is zero (or very close to it). For these measurements, a plug was placed in the end of the centrally located flow-through section 3.8 cm beyond axis of the focused microwave beam. The electrostatic probes were mounted on the plug face and stood 1.0 cm off the end wall (2.8 cm beyond the focused microwave beam in the box). For data analysis purposes it would have been desirable to locate both probes at the same axial position along the box in order to sample elements of test gas with identical histories behind the incident and reflected shocks at the points of measurement. This was not possible, however, because the electrostatic probes and their mounts would have seriously interfered with the focused probe measurements.

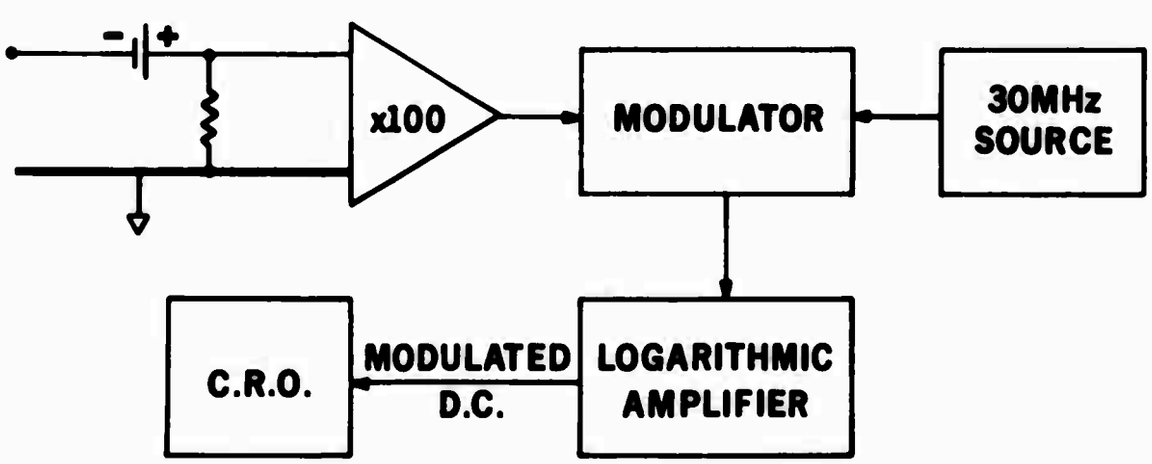

Figure 4 Block Diagram of Electrostatic Probe Electronics

Figure 5a shows oscilloscope traces for $A(t) \sin \theta(t)$ and $A \cos \theta(t)$ (i.e., electron density) taken in the reflected shock configuration. Figure 5b shows the electrostatic probe currents (on a linear vertical scale) from two probes for the same shot. The lower trace is for a spherical probe 0.76 mm in diameter biased at -15 volts; the upper trace is for a cylindrical probe. The undisturbed gas ahead of the shock is labeled region (1). Region (2) is the gas behind the incident shock which shows the rapid chemi-ionization and the slower recombination (Eq. (1)). Region (5) is the reflected shock region. The flow velocity of the gas is brought to zero; the temperature suddenly rises from $5,150^{\circ}K$ (i.e., T_2) to $9,100^{\circ}K$ (i.e., T_5) and chemi-ionization starts again, sending all the traces off scale. The electrostatic probes follow the electron density quite well.

B. SIMILARITY PARAMETERS AND CORRELATION OF SPHERICAL PROBE DATA

In order to calibrate a probe in conditions which do not precisely duplicate those where it is to be applied, it is necessary to establish the similarity parameters which govern the probe response. These can be found formally by dimensionless analysis. To facilitate this, the following observations can be made about the flow conditions in the present context:

(1) The flow about the probes was in or near the continuum regime in the ballistics range as well as in the shock tube where the calibration was performed.

(2) Although in the hypersonic wake the flow was turbulent (unsteady), the flow over the probes was assumed to be quasi-steady, which would be true if the probe diameter were small compared with a characteristic turbulent eddy size. Steady flow was established in the shock tube.

(3) The flow over the probes was, to a good approximation, chemically frozen in both test environments. The rate coefficient (α) for the dissociative recombination reaction (1) has been measured[10] over the temperature range $2,500^{\circ}-5,000^{\circ}K$ to be $\alpha = 1.08T^{-2} cm^3 sec^{-1}$. The characteristic plasma decay time, defined as $[d(\ln n_e)/dt]^{-1} = 1/\alpha n_e$, was thus found to be somewhat in excess of 100 μsec in the shock-tube experiments. Since this time was so much longer than the characteristic flow time over the probes ($< 1\mu$sec), the assumption of a chemically frozen flow was almost certainly justified even after allowance is made for the presence of a weak bowshock wave.

(4) The gas was weakly ionized.

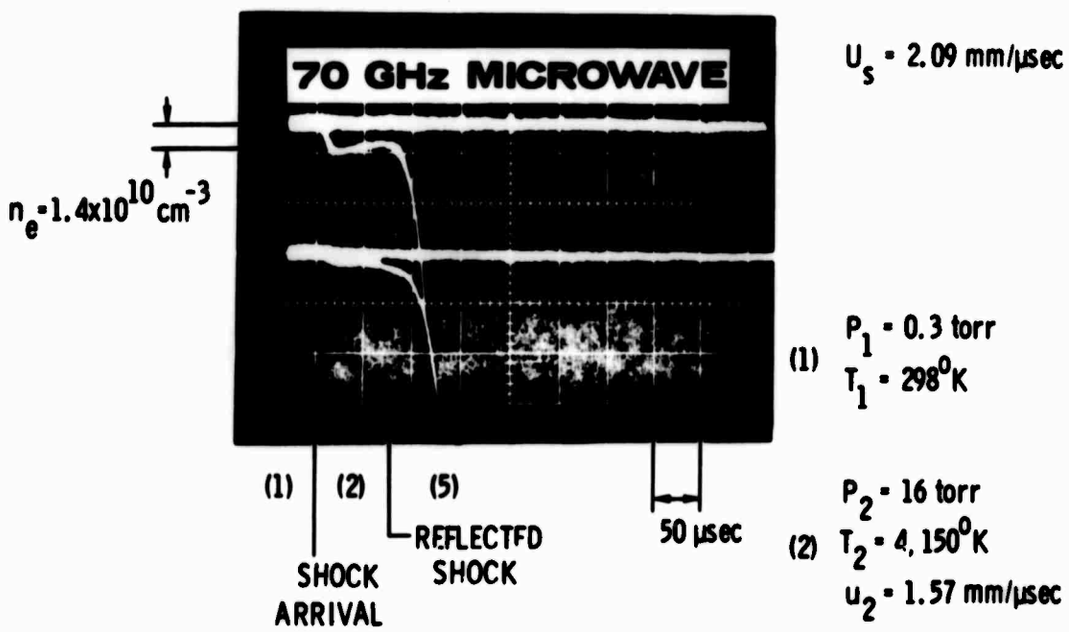

(a) Microwave Probe. Top trace A sin θ(t), lower trace A cos θ(t)

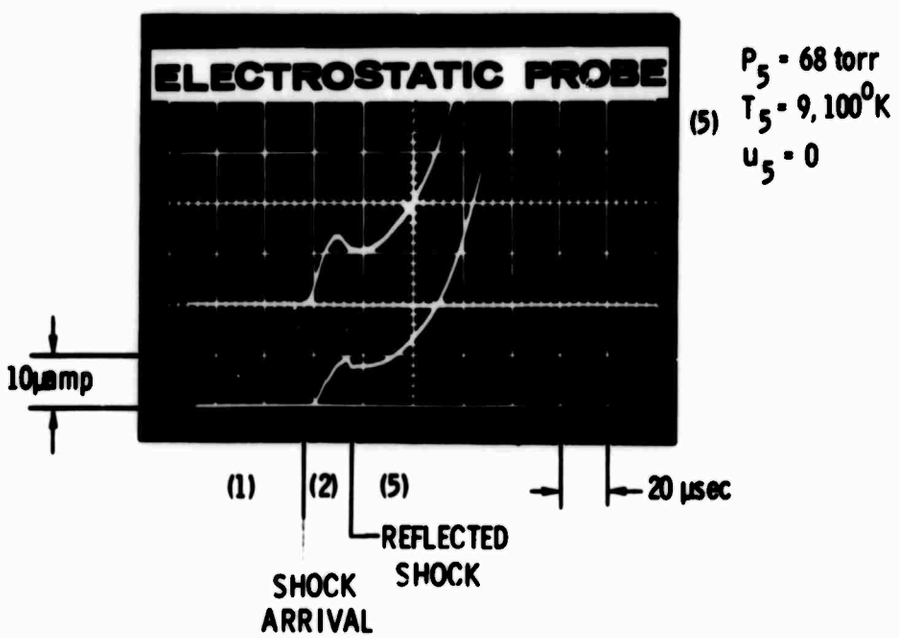

(b) Electrostatic Probes. Top trace cylindrical probe (⊥ to flow direction), lower trace spherical probe. Note different time bases between 5(a) and 5(b)

Figure 5 Response of Probes in Reflected Shock Region

Under such flow conditions the current drawn by a probe is governed by seven equations: the (frozen) ion and electron conservation equations, Poisson's equation, the conservation equations for mass, momentum, and energy, and the equations of state for the gas. The solution of these equations depends on the following physical quantities:

r	=	probe radius
V	=	potential of probe with respect to plasma
v_f	=	flow velocity of gas
ρ	=	gas density (local free-stream values)
υ	=	gas kinematic viscosity
T	=	gas temperature
n_i, n_e	=	ion and electron number densities in gas (assumed equal)
D_i, D_e	=	ion and electron diffusion coefficients
γ	=	ratio of specific heats of gas, Cp/Cv
T_w	=	probe wall temperature
m	=	molecular weight of gas
k, ϵ_o	=	Boltzmann's constant, premittivity of free space
e	=	electronic charge.

From dimensional analysis we find that eight independent dimensionless parameters can be formed from the above quantities:

Re	=	$v_f 2r/\upsilon$, Reynolds number based on probe diameter
λ_D/r	=	ratio of Debye length to probe radius, where $\lambda_D = \sqrt{e^2 n_e/\epsilon_o kT}$
ϕ	=	eV/kT, dimensionless probe potential with respect to the ionized gas
M	=	$v_f/\sqrt{\gamma RT}$, Mach number, where R is gas constant per unit mass
γ	=	ratio of gas specific heats
Sc	=	υ/D_i, Schmidt number based on ion diffusion coefficient
D_i/D_e	=	ratio of ion and electron diffusion coefficients
T_w/T	=	dimensionless probe wall temperature.

It follows that if we define a dimensionless probe current i,

$$i = \frac{Ir}{e n_i D_i (4\pi r^2)} \qquad (2)$$

where

I = total current drawn by probe,

then this dimensionless current must be a function only of the eight dimensionless parameters listed above, i.e.,

$$i = i(Re, \lambda_D/r, \phi, M, \gamma, Sc, D_i/D_e, T_w/T) \tag{3}$$

We note that i is simply the Nusselt number (Nu) for mass transfer (often called the Sherwood number and denoted by Sh in the chemical literature).

The object of a calibration is to measure the dimensionless current i at conditions where the similarity parameters on which it depends have the same values as in the environment where the probe is to be applied; hopefully, by covering a sufficiently wide range of the parameters, the functional relationship for i can be inferred from the results.

In the general case, the function i obviously contains too many variables to yield readily to such an approach. Fortunately, in many circumstances several of the eight parameters in Eq. (3) are either of secondary importance or essentially invariant. For example, $Sc \approx 1$ for all gases. Furthermore, if we confine our attention to the collection of ions at relatively high negative probe potentials, the electron diffusion coefficient should not influence the problem significantly ($D_i/D_e \approx 0$). The parameter T_w/T was also assumed to be of secondary importance (its value in these experiments, where the probes remained at essentially room temperature, was small). The insensitivity of i to T_w/T was confirmed by the experiments. This is to be expected in conditions where the boundary layer (i.e., the region in which the influence of the wall temperature could be important) is thinner than the sheath. This was the case in the present experiments, as will be discussed below. Finally, in a low subsonic flow the ion collection would also be insensitive to the Mach number and the specific heat ratio, and the essential parameters would thus be reduced to three in number, i.e.,

$$i \cong i(Re, \lambda_D/r, \phi) \tag{4}$$

It is the functional form of this relationship that we sought to establish experimentally. It should be pointed out, however, that although over the major portion of the wakes in the ballistics range the flow was indeed subsonic, the calibration experiments were performed in a shock tube where the Mach number M_2 seen by the probes

ranged from 1.1 to 1.4 – i.e., it was essentially constant at a low supersonic value. However, based on existing analyses of supersonic blunt probes (e.g., References 6 and 7) it appears reasonable to assume that at such modest Mach numbers, the flow dependence of the ion collection is felt primarily through the Reynolds number rather than the Mach number. The very small range of Mach numbers available in the shock tube (behind the incident shock) prevented a direct check on this point. However, reflected shock measurements (discussed later) where the Mach number was zero does confirm this point. In addition, a subsequent application of the calibration in the ballistic range (see Section III), where the Mach number ranged to very low subsonic values, yielded good agreement with microwave measurements of electron density and thus the assumption of Mach number independence appears to be well supported.

The calibration procedure in the shock tube was as follows. For given flow conditions ($Re, \lambda_D/r$) and probe potential (ϕ), the probe current (I) and electron-ion number density (n) were measured independently, as described in Section IIA, and i was calculated. The procedure was repeated for as wide a range of flow conditions as possible so as to map out the functional form of Eq. (4).

The pressure, temperature, and flow velocity of the test gas were calculated from normal shock-wave relations. The ion diffusion coefficient was calculated for 4,000°K from the cross-section data of Hirshfelder, Curtiss, and Bird[18] (for OH_3^+ in Ar, it was 9810/p cm^2 sec^{-1} with p the pressure in torr) and extrapolated to other temperatures with the assumed dependence[19] $D_i \sim T^{1.75}/p$. A problem which was encountered was the determination of the potential of the plasma, relative to which the probe potential was to be specified. The floating potential of the probes in the shock tube (i.e., the potential where the net current was zero) was established to be within about 1/2 volt of the shock-tube ground. The plasma potential is somewhat positive with respect to the floating potential,[4–6] the difference being of the order kT/e (0.2 to 0.5 volt in the shock-tube experiments), the precise value depending on the particular flow conditions. All the voltages referred to in this report were measured with respect to the shock-tube ground on the assumption that the difference between it and the plasma potential was small compared with the applied voltage.

Some results from the calibration are shown in Figures 6 through 9. The approach was to try to infer from data of this sort an analytic expression for $i(Re, \lambda_D/r, 0)$ which would satisfactorily correlate all the data.

Figure 6 shows typical data of i as a function of Re for three values of probe potential, with λ_D/r in the range 4×10^{-2} to 9×10^{-2} for all points. Data of this sort suggested that i may be described by the form

$$i = f(\emptyset, \lambda_D/r)\ (a+bRe^{\beta}) \tag{5}$$

where f is an increasing function of $\emptyset$, and a, b, and β may depend on λ_D/r. Figure 7 shows measurements of i as a function of $\emptyset$ at a fixed Reynolds number and λ_D/r. This and similar data suggested that the potential dependence could be modeled in the form

$$f(\emptyset, \lambda_D/r) = (-\emptyset)^{\alpha(\lambda_D/r)} \tag{6}$$

where α is a function of λ_D/r. (Note that $\emptyset$ is negative.) α was determined from plots like the one shown in Figure 7. The results are shown in Figure 8. The points are fitted with the analytic relation

$$\alpha = \frac{1}{1+0.61\ ln(1+r/\lambda_D)} \tag{7}$$

which was chosen so as to not only fit the data but to extrapolate to the expected theoretical limits $\alpha \to 0$ for $\lambda_D/r \to 0$ (see Ref. 20) and $\alpha \to 1$ for $\lambda_D/r >> 1$ (see Refs. 5, 20) at the lower Reynolds numbers.

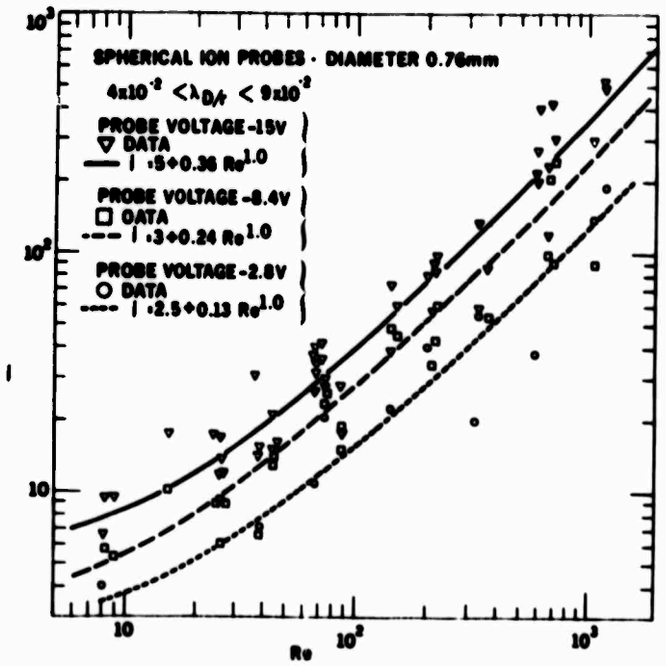

Figure 6 Shock Tube Calibration, i vs Re for Three Probe Voltages: V = -2.8 volts ($\emptyset$=7 to -13), V = 8.4 Volts ($\emptyset$ = -21 to 38) and V = -15 ($\emptyset$ = -38 to -70)

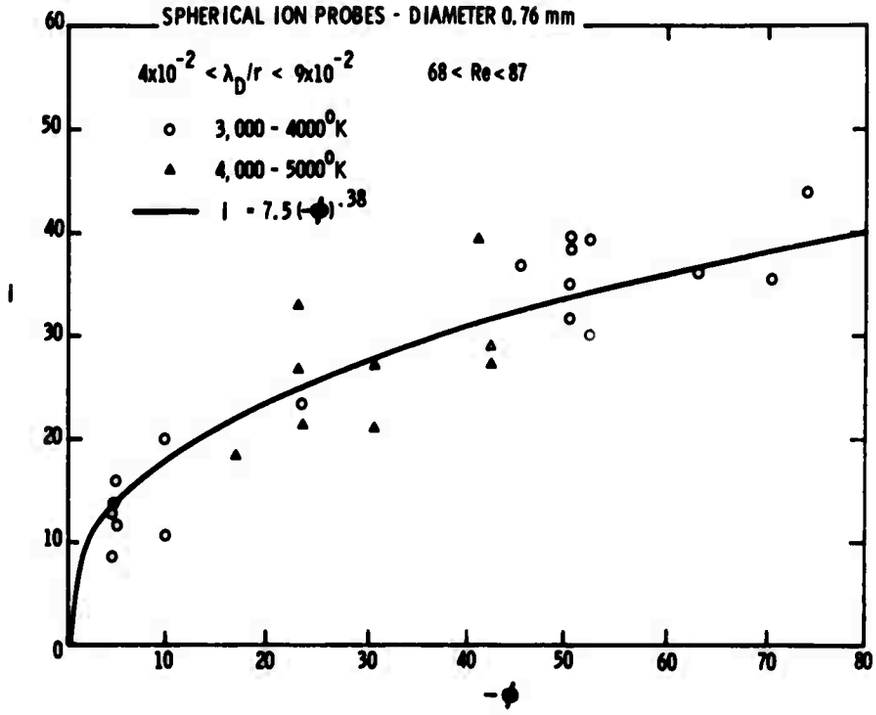

(a) $\lambda_D/r = (6 \pm 3) \times 10^{-2}$ Re = 78± 10

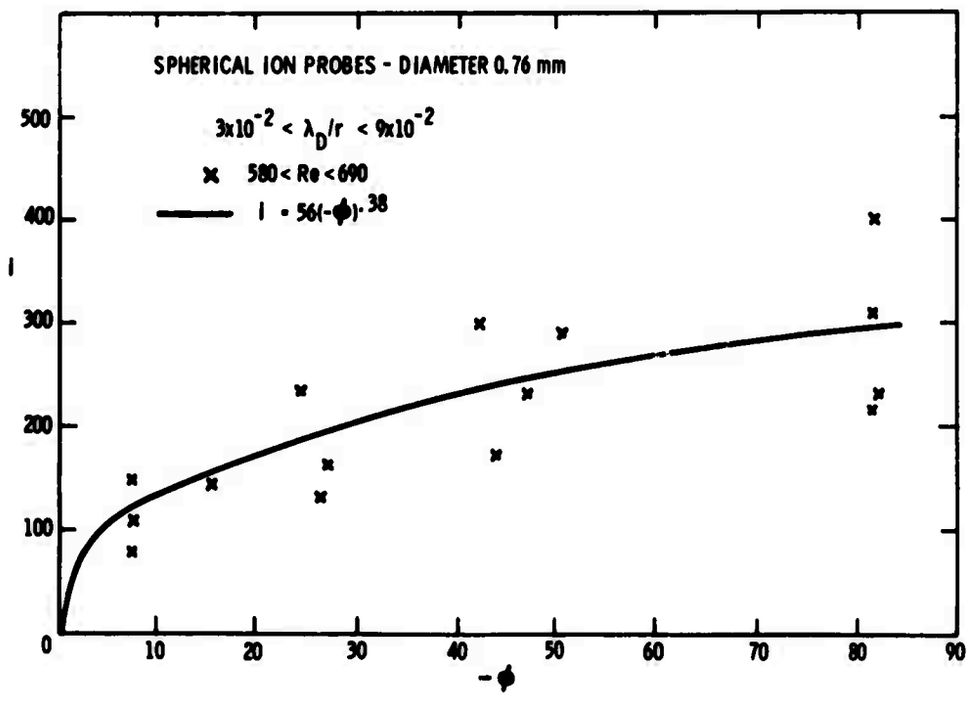

(b) $\lambda_D/r = (6 \pm 3) \times 10^{-2}$ Re = 635± 55

Figure 7 Dependence of i on Probe Potential ø

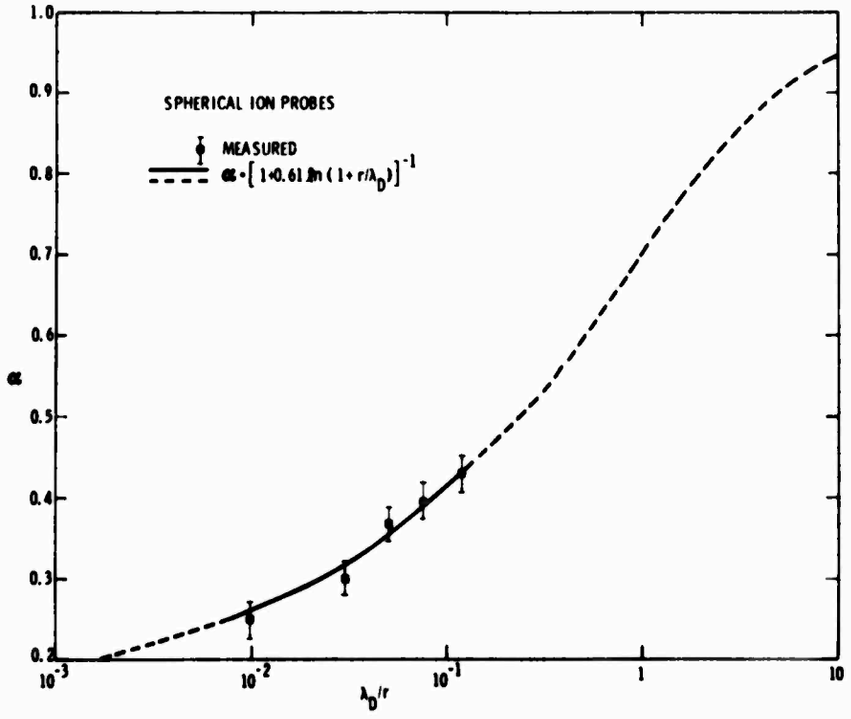

Figure 8 Shock Tube Calibration of α as a Function of λ_D/r

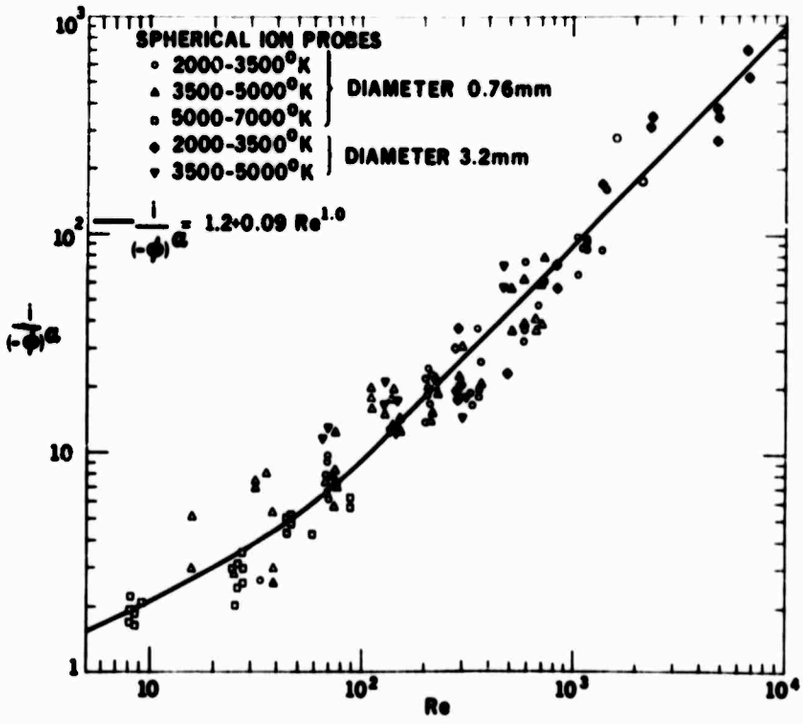

Figure 9 Correlation of Shock Tube Data in Terms of Equation (8)

It was found that, to a good approximation, a, b, and β in Eq. (5) could be regarded as independent of λ_D/r and all the results covering the range of parameters: $4 < Re < 10^4$, $10^{-2} < \lambda_D/r < 0.15$, $-10^2 < \phi < -10$, correlated with the relation:

$$i = (-\phi)^{\frac{1}{(1+0.61\ln(1+r/\lambda_D)}} \left[1.2 + 0.09\ Re^{1.0}\right] \qquad (8)$$

Figure 9 shows Eq. (8) together with all the experimental data plotted in the same form. Clearly, the correlation appears to be reasonably successful. The data fits with an average scatter of less than 50% and shows no systematic deviation from the correlation curve.

Only incident shock measurements were used to obtain Eq. (8) and the value of 1.2 was obtained by extrapolation of the data to $Re \to 0$. The reflected shock data, on the other hand, is (in principle) capable of giving a more accurate value since no extrapolation is required because Re is zero (or very close to it). Also, since M is zero, its influence on i can be checked.

For the reflected shock measurements the probe diameter was 0.76 mm and bias -15 volts. Since the focused and electrostatic probes were located at slightly different axial positions in the test box, data obtained behind the reflected shock are the result of different gas histories behind the incident shock. Therefore, there could be no point-to-point comparison between the microwave and electrostatic probes. Instead, the electron density behind the reflected shock was determined as follows: The time of arrival, Δt, of the reflected shock behind the incident shock at the electrostatic probe was determined from the trace in Figure 5b. The electron density behind the reflected shock at the electrostatic probe was then calculated by multiplying the electron density behind the incident shock at the microwave probe at time Δt (see Figure 5a) by the density ratio ρ_5/ρ_2.

Two processes are operative around the electrostatic probes behind the reflected shocks. First, the flow velocity does not instantaneously go to zero behind the reflected shock. Fluctuations caused by interactions of the shock with the probe damp out in a time of the order r^2/υ (equal to 7μsec for the conditions in Figure 5). During this damping period the probe currents reach a minimum as $Re \to 0$ and then increase due to an increase in ionization as a consequence of the increased temperature behind the reflected shock. This increase is seen in all the traces (Region (5) in Figures 5a and b).

Thus the method of data reduction is not exact but should yield a reasonably good approximation to i for Re and M equal to zero. Reflected probe data so treated yields a value of $i = 6.3$ compared to 5 obtained from the incident shock measurements for Re extrapolated to zero (see Figure 6). A corresponding value of $i/\phi^{\alpha} \cong 2.2$ (with α obtained from Figure 8 – i.e., we assume to Re-dependence of α) was obtained behind the reflected shock compared to the incident shock's extrapolated value of 1.2 (see Figure 9). It is of interest to note that the former value is closer to the theoretical value (see next section) than the latter. However, both are in reasonable agreement with theory. The most valuable result of the reflected shock measurements is that they confirm the Mach number dependence of i to be small, as was originally supposed.

C. DISCUSSION AND COMPARISON WITH AVAILABLE THEORY

Since no theoretical results are available for spherical probes for the conditions of the experiments described here, a direct comparison of Eq. (8) with theory cannot be made. It is interesting to examine, however, whether Eq. (8) reduces to the theoretically predicted forms when extrapolated to the limits for which explicit solutions are available.

First, consider the limit of a static probe, $Re \to 0$. The theory of Su and Lam[20] for spherical probes yields $i = 2$ for $\lambda_D/r \to 0$, and $i = (-\phi)$ for $\lambda_D/r >> 1$ (for the latter limit, see also Hoult[5]). The correlation equation, Eq. (8), reduces to $i = 1.2$ and $i = -1.2\phi$, respectively, in these limits. This agreement is quite satisfactory, particularly since the data did not extend to sufficiently low Reynolds numbers to warrant confidence in an extrapolation to $Re \to 0$, and since in any practical situation the number density in the vicinity of a static probe (and hence the current to it) will be depressed from the ideal value because of diffusion to the probe supports. The reflected shock data gave $i = 2.2$ and $i = -2.2\phi$, respectively, in the above limits. This data does, however, suffer from approximations in the data reduction process.

An extrapolation of Eq. (8) to high Reynolds numbers, on the other hand, does not yield agreement with the theories available for the limits $\lambda_D/r \to 0$ and $\lambda_D/r >> 1$. Lam's laminar theory[4] for $Re >> 1$ predicts $i \sim Re^{1/2}$ in the limit $\lambda_D/r \to 0$, whereas Eq. (8) extrapolates to $i = 0.09\, Re^{1.0}$. For $\lambda_D/r >> 1$, Sonin's theory[6] predicts $i \sim Re^{1/2}$ for $(-\phi) << Re^{1/2}$ and $i \approx (-\phi)$ for $(-\phi) >> Re^{1/2}$, again in disagreement with Eq. (8).

This disagreement is not surprising. The correlation equation is an approximate one which was chosen to fit as well as possible all data obtained over the range of conditions of these experiments (Figure 1). The function i of Eq. (8) is actually a very complex one at high Re, as evidenced by the wealth of theories which the electrostatic probe problem has spawned, and there is no reason to expect that the approximate correlation would not break down outside the region where it was obtained. For example, Lam's theory[4] yields $i \sim Re^{1/2}$ only in the limit where the electrostatic sheath is thin compared with the boundary layer thickness, and Sonin's theory[6] is for the case of very large λ_D/r where the probe is unsheathed. In these experiments, on the other hand, the sheath was large compared with the boundary layer thickness except at low Re, and comparable, in fact, with the probe radius (but never large compared with r). An approximate analysis has been given by Boer and Johnson[21,22] for ion collection by a flat plate probe under conditions where the sheath is thick compared with the boundary layer. Their result can be written in the form

$$i \sim (\lambda_D/r)^{1/2} (-\phi)^{1/2} Re^{3/4}. \qquad (9)$$

A quite similar result is obtained if their approach is applied to ion collection in the stagnation-point region of a sphere or a cylinder (see Appendix B), with the assumption that the sheath is thick compared with the boundary layer but thin compared with the body radius (the difference resides only in a constant, which has, in any case, been omitted from the equation quoted above). The above equation does not agree well with the present experiments, where the sheath was estimated to be not only thicker than the boundary layer, but often comparable with the probe radius. Numerical computations for flat probes with thick sheaths have also been performed by Dukowicz.[23] In a certain range of λ_D/r and Re, Dukowicz correlates his computed results with a formula which in our notation reads $i \sim (-\phi)^{1/2} Re^{1/2}$. Dukowicz also shows experimental data for slender conical probes which he fits with the relation $i \sim (-\phi)^{0.3} Re^{0.7}$. An extension of his theory to spherical probes with thick sheaths would be of interest in the present context.

A point of interest is that in the limits $Re >> 1$ and $\lambda_D/r \to 0$, our correlation equation, Eq. (8), implies that:

$$I = 0.9\, en\, v_f\, (\pi r^2) \qquad (10)$$

i.e., that the collected current is essentially equal to the flux of ions "swept out" of the flow by the cross section of the probe. Noting next that the flow velocity was

close to the average thermal speed $\bar{v}_{th}$ of the ions at low supersonic Mach numbers, we see that the same equation can be rearranged to yield

$$I \approx \frac{en\bar{v}_{th}}{4} (4\pi r^2) \qquad (11)$$

One would, indeed, anticipate a relation like (10) for a probe in a hypersonic, collision-free flow, and a relation like (11) for a probe in a stationary, collision-free plasma. That they both happen to be implied simultaneously by an experimental correlation formula obtained at continuum-flow conditions (mean free path/probe radius from 10^{-4} to 10^{-1}) at high Re and $M \approx 1$ should not, necessarily, be taken to mean that the mechanism of ion collection in continuum flows is either the "sweeping out" of ions from the flow or their arrival at the probe by simple random, collision-free flux.

Expressions of the type shown in Equations (10) and (11) have been used[24,25] to reduce electrostatic probe data in continuum flowing plasmas when $\lambda_D / r << 1$. In hypersonic wakes, however, the latter condition is not met and, in addition, v_f is generally much smaller than $\bar{v}_{th}$. The full calibration (Equation (8)) then must be used. The factor $(-\phi)^{\alpha}$ is, of course, related to the sheath size, which may be thought of as increasing the collection area of the probes. Incidentally, Renau and Scharfman[26] have pointed out that our values of ϕ^{α} (which range from 1.4 to 7) are quite close (within 25%) to $(s/r)^2$. Here s is the sheath radius and may be estimated from either the work of Su and Lam[20] or Travers and Williams.[27] (Both references have expressions for s which give numbers within 25% of each other.)

The following section describes work where the empirical calibration formula, Equation (8), was used to interpret spherical probe data taken in the wakes of hypersonic projectiles. As shall be seen, good agreement was obtained with microwave measurements over several orders of magnitude in electron density (despite, we note, the difference in Mach number in the two environments). This leaves us with some confidence that our calibration technique is successful and accurate to perhaps ±50%.

III. APPLICATION TO HYPERSONIC WAKES

An array of twelve spherical electrostatic probes was installed in AC-DRL's ballistics range to map electron and ion density distributions behind hypervelocity projectiles (see Figure 10). The calibration of the previous section was then used to calculate ion density distributions in the wake from the mean current collected by the ion probes. For purposes of computation we set $\upsilon/D_i = 0.8$ and rearranged Equation (8) in the form

$$I = (-\phi)^{\alpha}\, en\,(4\pi r^2)\,(1.2\, D_i/r + 0.225\, v_f)\,. \qquad (12)$$

The profiles of temperature and wake velocity used were those calculated by Wen[28] which are in essential agreement with the measurements made at CARDE.[29] The Debye length was estimated from the electron density measured by microwave techniques.[9,30]

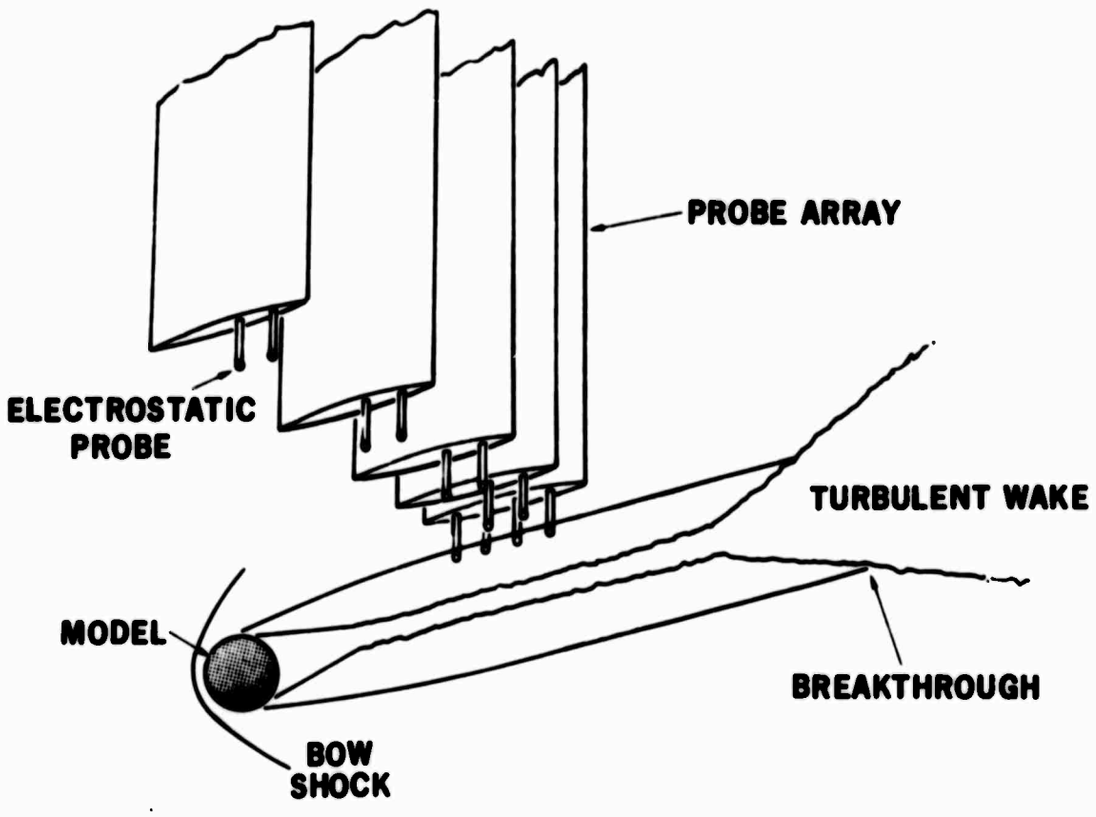

Figure 10 Electrostatic Probes in Free-Flight Range

Figure 11 shows an example of a radial ion density distribution obtained from probe measurements. Most of the data at large R/D is for 5mm spheres and that at small R/D is for 15mm spheres. (R is the distance from the probes to the wake center, and D the sphere diameter.) Since it is observed that the fluid wake width[31] scales with D and that $n_e D_p$ (the line integral of n_e across the wake) is approximately constant at a given pD, the ion density for the large sphere has been multiplied by three to allow a direct comparison in Figure 11. The profile can, to a good approximation, be fitted with a Gaussian curve.

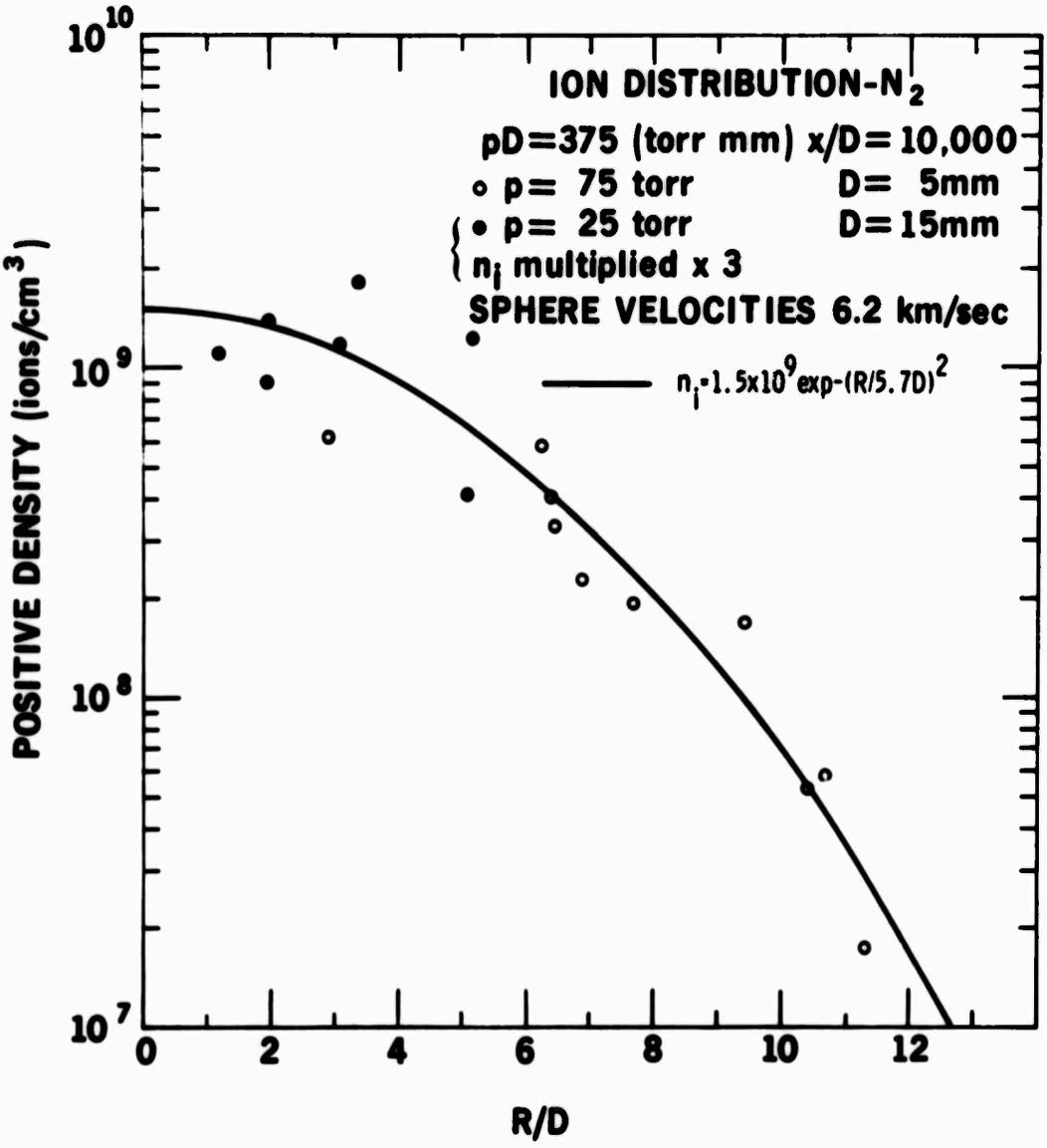

Figure 11 Radial Distribution of Ion Density in Nitrogen Wake

The ion density n_i of Figure 11 and for other x/D (ratio of distance behind model to model diameter) has been integrated over the wake diameter to give $n_i D_p$ (D_p may be thought of as an equivalent plasma "diameter"). These computations are compared in Figure 12 with the integrated electron density $n_e D_p$ as measured with microwave probes and resonators.[9,27] Note that, although the product $n_i D_p$ changed only modestly in the measurements, the corresponding change in n_i was about three orders of magnitude. The agreement is good considering that the wake is very turbulent and our knowledge of even its mean properties (such as v_f and T) is very imperfect.

The wakes studied in the free-flight range sometimes use mass addition to either increase or decrease the electron concentration. Under these circumstances, calibrated electrostatic probes can be used as an aid in wake chemistry studies. For example, Figure 13 shows the positive ion density calculated from the average probe current measurements obtained in the wake of a 15mm sphere which injected freon into the wake. Also shown is the electron density n_e measured with microwave probes. Assuming charge neutrality, the difference between these two curves is the negative ion concentration n_-. These measurements indicate that attachment of electrons to form negative ions was very rapid. On the other hand, charge neutralization between ions was very slow.

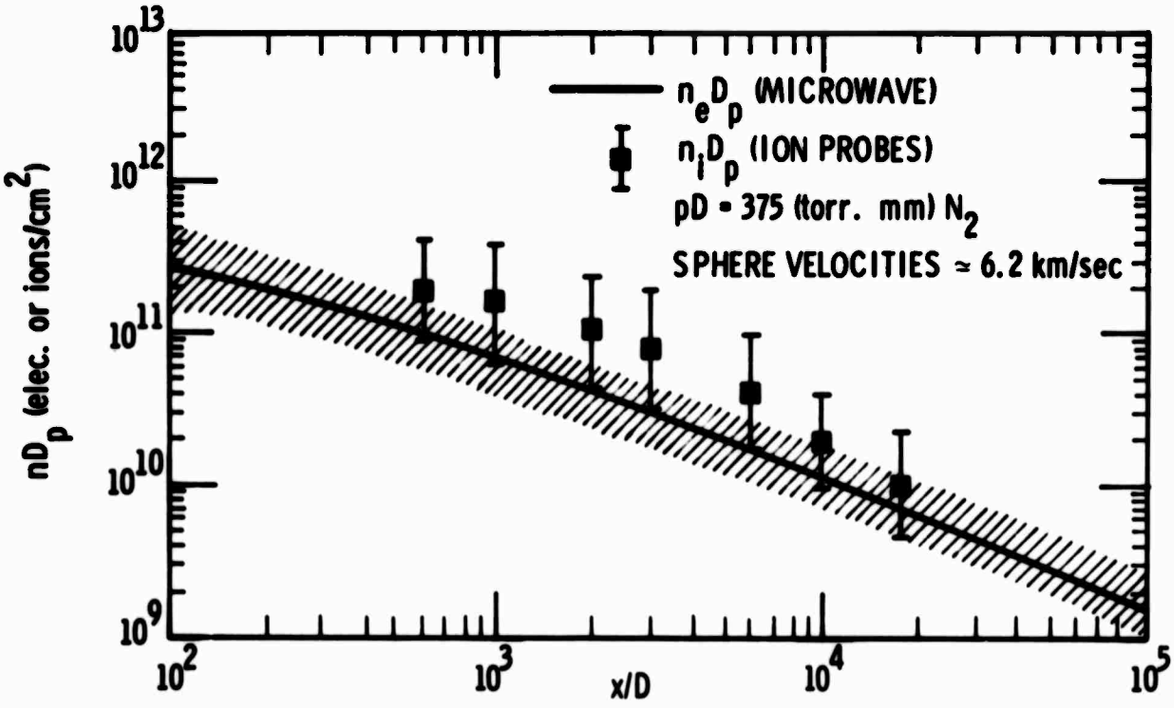

Figure 12 Comparison of Integrated Ion Density (Electrostatic Probes) and Integrated Electron Density (Microwave Probes)

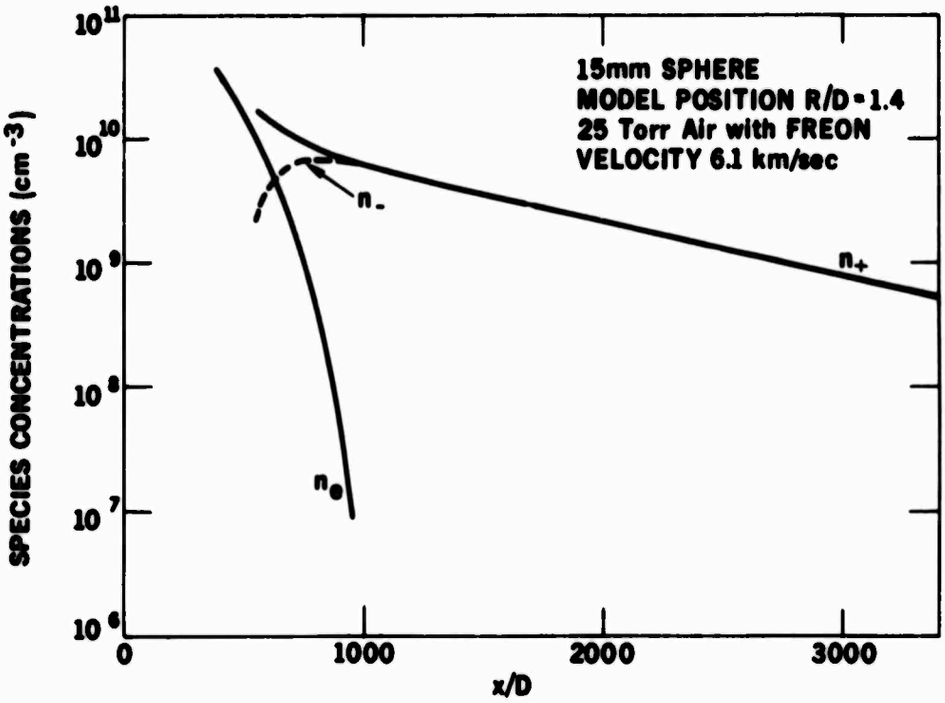

Figure 13 Application of Calibration to Wake Seeded with Freon

IV. SUMMARY

The present work demonstrates that the continuum electrostatic probe is a useful instrument for making point measurements of charge density in the wakes of hypervelocity projectiles. Difficulties encountered from lack of an accurate theory for probe operation in the conditions of a typical ballistics range were overcome by a calibration of spherical, ion-collecting probes in a shock tube. From this calibration, an analytic correlation formula (Eq. (8)) was obtained for the probe current as a function of the appropriate similarity parameters over a wide range of conditions. This empirical correlation equation was used to interpret the readings of probes arranged in the wakes of hypersonic projectiles in the ballistics range. Axial and radial profiles of charged particle density were obtained. The results were in good agreement with microwave measurements of integrated electron density.

REFERENCES

1. W. M. Kornegay, AIAA J. 3, 1819 (1965)
2. R. A. Hayami and R. I. Primich, in AGARD Conference Proc., No. 19, May 1967
3. G. W. Sutton, AIAA J. 7, 193 (1969)
4. S. H. Lam, AIAA J. 2, 256 (1964)
5. D. P. Hoult, J. Geophys. Res. 70, 3183 (1965)
6. A. A. Sonin, J. Geophys. Res. 72, 4547 (1967)
7. C. H. Su, AIAA J. 3, 842 (1965)
8. S. Zivanovic, P. E. Robillard, and R. I. Primich, in AGARD Conference Proc. No. 19, May 1967
9. R. I. Primich, D. H. Auston, R. A. Hayami, J. D. McLeod and S. Zivanovic, in Proc. of Seventh International Conference on Phenomena in Ionized Gases, Vol. III, 128 (1966)
10. L. N. Wilson and E. W. Evans, J. Chem. Phys. 46, 859 (1967)
11. J. A. Green and T. M. Sugden, Proc. of Ninth Symposium on Combustion, p. 607 (1963)
12. H. F. Calcote et al., Proc. on Ninth Symposium on Combustion, p. 622 (1963)
13. G. P. Glass, et al., J. Chem. Phys. 42, 608 (1965)
14. R. I. Primich and R. A. Hayami, GM-DRL Report TR63-217C, Jul 1963
15. M. Born and E. Wolf, Principles of Optics, Pergamon Press, New York, 1959
16. R. I. Primich and F. H. Northover IEEE Trans. AP-11, (1963)
17. S. Zivanovic, H. M. Musal, and R. I. Primich, IEEE Trans AP-12, 618 (1964)
18. J. O. Hirshfelder, C. F. Curtiss, and R. B. Bird, Molecular Theory of Gases and Liquids, Wiley (1964)
19. A. Dalgarno, "Diffusion and Mobilities" in Atomic and Molecular Processes, Ed. D. R. Bates, Academic Press (1962)
20. C. H. Su and S. H. Lam, Phys. Fluids 6, 1479 (1963)
21. P. C. T. deBoer and R. A. Johnson, Phys. Fluids 4, 909 (1968)
22. P. C. T. deBoer, R. A. Johnson, and W. P. Thompson, AIAA Paper No. 68-165
23. J. K. Dukowicz, in Record of International Congress on Instrumentation and Aerospace Simulation Facilities, p. 52, 1969, also Cornell Aeronautical Laboratories Report RA-2641-Y-1, Jan 1969
24. W. E. Sharfman et al., in Proc. of Third Symposium on the Plasma Sheath, Vol. II, Spartan Book Co., N. Y., 1967

25. T. I. McLaren and R. M. Hobson, Phys. Fluids. 11, 2162 (1968)
26. J. Renau and W. Scharfman, Discussion at Stanford Research Institute 27 Feb 1969
27. B. E. L. Travers and H. Williams, Tenth Symposium (International) on Combustion, p. 657, 1968
28. K. S. Wen, T. Chen and B. Lieu, AC-DRL Report TR68-01D, Jun 1968 also AIAA Preprint 68-702
29. --- "Reentry Physics Research Program in Turbulent Wakes," CARDE Semiannual Progress Report, Jun 1968
30. R. A. Hayami and K. J. Kelly, IEEE Trans. AES-3, 339 (1967)
31. L. N. Wilson, AIAA J. 5, 1' (1967)
32. H. Schlichting, Boundar' ayer Theory, McGraw-Hill (1960)

BLANK PAGE

APPENDIX A
CALIBRATION OF CYLINDRICAL ELECTROSTATIC PROBES IN A CONTINUUM PLASMA FLOW

Most of the work in this report is concerned with spherical probes, which are insensitive to flow direction and for that reason have perhaps the simplest geometry for the measurement of ion density in turbulent flow conditions. There are also, however, many applications for probes of other geometries which are sensitive to the flow direction. In this appendix are presented some results from a calibration of cylindrical probes in continuum flow conditions simulating the typical existing ballistics range environment. Only ion collection is considered. The data presented here covers a fairly limited range of the similarity parameters which govern probe response, and does not represent a complete calibration of cylindrical probes. Nevertheless, it has some fundamental interest, and is pertinent to applications in the ballistics range.

The experiments were performed with the apparatus described in Section II in the main body of this report. Again, the calibration involved the comparison of simultaneous measurements of ion current with probes and electron density with a focused microwave system. Two cylindrical probe geometries were employed. The probes aligned with the flow had a radius of 0.11mm and length of 20mm, while those oriented with their axes perpendicular to the flow had a radius of 0.15mm and length of 20mm.

The probe calibration is again expressed in terms of a dimensionless probe current i (which is essentially the Nusselt number for ion transfer)(c.f., Eq. 2)

$$i = \frac{Ir}{en_i D_i \cdot 2\pi r \ell} \qquad \text{(A-1)}$$

where r is the probe radius, and ℓ is the probe length. The dimensionless current is primarily a function of four dimensionless similarity parameters, (c.f., Eq. 4)

$$i = i(Re, \lambda_D/r, \emptyset, \ell/r) \qquad \text{(A-2)}$$

where $Re = \frac{v_f 2r}{\nu}$ is the Reynolds number based on probe diameter, λ_D/r is the ratio of Debye length to probe radius, $\emptyset = eV/kT$ is the dimensionless probe potential, and ℓ/r is the probe length to radius ratio.

Note that if $\ell/r >> 1$, i will be independent of ℓ/r for a probe perpendicular to the flow, but not for a probe aligned with the flow. This is because the boundary layer (and the sheath) scales with r for a perpendicular probe, but with ℓ for an aligned probe.

Theoretical solutions for the dimensionless probe current of Eq. (A-2) are available, or can be derived by means of available techniques, only for certain limiting cases. Lam[4] deals with the case of a thin laminar boundary layer in the limit $\lambda_D/r \to 0$ (sheath << boundary layer << probe size), where the ion collection is controlled by diffusion across the boundary layer and is essentially independent of probe potential. For a cylindrical probe perpendicular to the flow, such an analysis yields

$$i \sim Re^{1/2} \tag{A-3}$$

while for a cylinder aligned with the flow, one obtains

$$i \sim (\ell/r)^{-1/2} Re^{1/2}. \tag{A-4}$$

An approximate solution for the case where the sheath is thick compared with the boundary layer, but thin compared with the probe dimensions (boundary layer << sheath << probe size) has been given by deBoer et al,[21,22] for a flat-plate probe. Their method of solution is extended in Appendix B to cylindrical probes oriented perpendicular to the flow velocity. An analytic solution is given in Eq. (B-5) for the dimensionless current i, based on the current density at the stagnation point of the cylinder, as a function of Re, λ_D/r, and ϕ.

In the present experiments, the sheath was of the order of the probe radius, and hence neither of the theories mentioned above are strictly applicable. In view of the absence of a more appropriate theory, however, they do offer a basis of comparison.

In our experiments, the Reynolds number was varied over three orders of magnitude, from about 1 to 10^3. The dependence of i on λ_D/r and ϕ, however, was explored only qualitatively, since the measurements involved only two values of each of these parameters for each probe orientation. The aspect ratio ℓ/r was kept fixed.

Figures A-1a,b,c, and d show results for the calibration of a probe perpendicular to the flow direction, in the form of a plot of i versus Re. The data are grouped according to λ_D/r and ϕ, with Figure A-1a having the larger values of these quantities

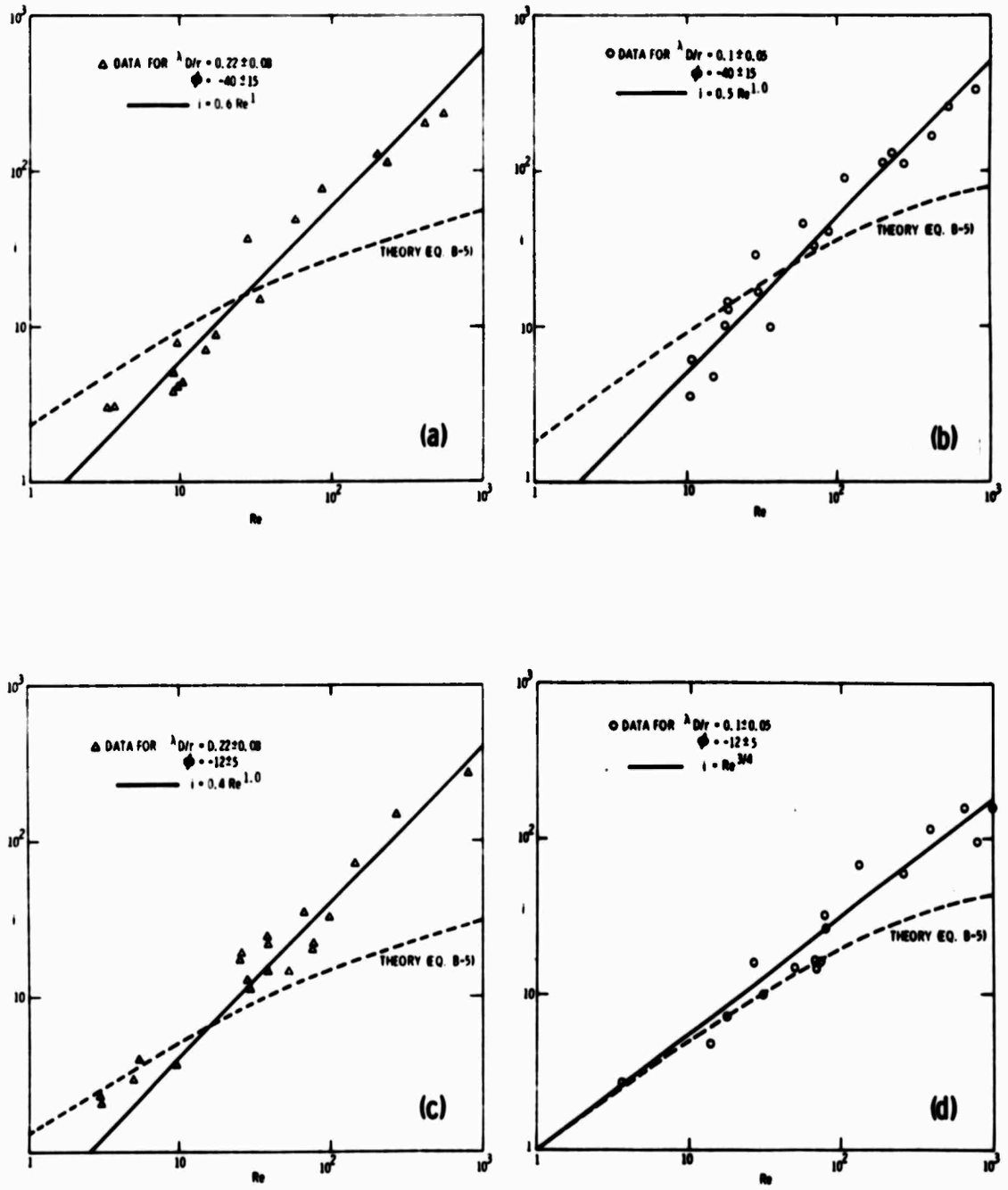

Figure A-1 Calibration of Cylindrical Probe Perpendicular to Flow (Radius r = 0.15mm, Length ℓ = 2.0mm)

and Figure A-1d the smaller. The indicated spread in the latter two quantities (for example $\phi = -40 \pm 15$) does not represent an inaccuracy of measurement, but merely reflects the grouping of experimental data. Each set of data points has been fitted with a simple relationship of the form $i = ARe^{\beta}$. The data of Figures A-1a, b, and c show that the exponent $\beta = 1$ gives a reasonable fit to the data just as in the case of spherical probes under similar conditions. The constant A is 0.6, 0.5, and 0.4 for Figures A-1a, b, and c respectively. The data of Figure A-1d is better fitted with an exponent of 3/4, however.

The data in Figure A-1 is not in good agreement with the theory for sheaths which are thin compared with the probe radius, as outlined in Appendix B. Equation B-5 predicts that i (at the stagnation point) should be proportional to Re to a power between 3/4 and 1/4, depending on ϕ and λ_D / r.

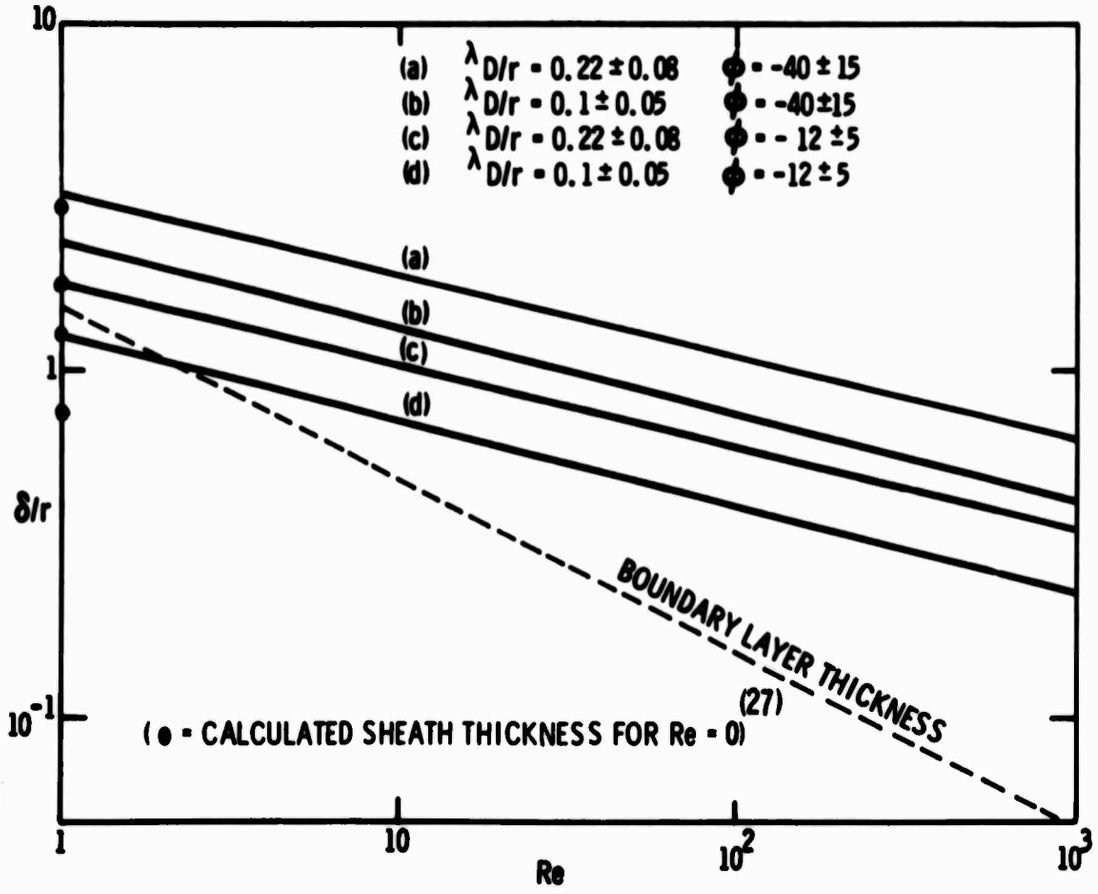

Figure A-2 Ratio of Sheath Thickness to Probe Radius δ/r for Cylindrical Probe Perpendicular to Flow. Also Boundary Layer Thickness

The disagreement may be due in large part to the fact that in the experiments the sheath thickness (calculated from Eq. (B-7) and shown in Figure A-2) was not small compared with the probe radius, as assumed in theory. For example, for the case, $\emptyset = -40$, and $\lambda_D/r = 0.22$, we estimate that the sheath thickness is about one probe radius at $Re \sim 10^2$, while for $\emptyset = -12$, and $\lambda_D/r = 0.1$ (Figure A-1d) it is about one-half the probe radius. (The viscous boundary layer thickness at the same Reynolds number is about 0.15 of the probe radius.) Note, however, that for the case with the thinnest sheath (lowest $\emptyset$ and λ_D/r), $i \sim Re^{3/4}$ rather than Re^1, i.e., the data appears to agree somewhat better with the thin-sheath theory than in the case of thicker sheaths. As expected, the current appears to increase somewhat with increasing $\emptyset$ and λ_D/r, although the increase is small in these cases and almost masked by data scatter.

Some results from the calibration of probes aligned with the flow direction are shown in Figure A-3. Here, the dimensionless current is to a good approximation proportional to $Re^{1/2}$, as predicted by the diffusion-controlled theory (Eq. (A-2)), but there is nevertheless a significant dependence on both λ_D/r and $\emptyset$, the current increasing with both these parameters. The data correlates well with the equation (see Figure A-4).

$$i = 0.45\,(\lambda_D/r)^{1/3}\,(-\emptyset)^{1/2}\,Re^{1/2}. \qquad \text{(A-5)}$$

These results are qualitatively consistent with a situation where the sheath is thinner than the boundary-layer thickness (leading to a basically $Re^{1/2}$ dependence) but not negligibly thin in comparison with it. For example, the sheath thickness has been estimated to be of about one probe radius, while at $Re = 10^2$, the boundary layer thickness is a few probe radii for an aligned probe.

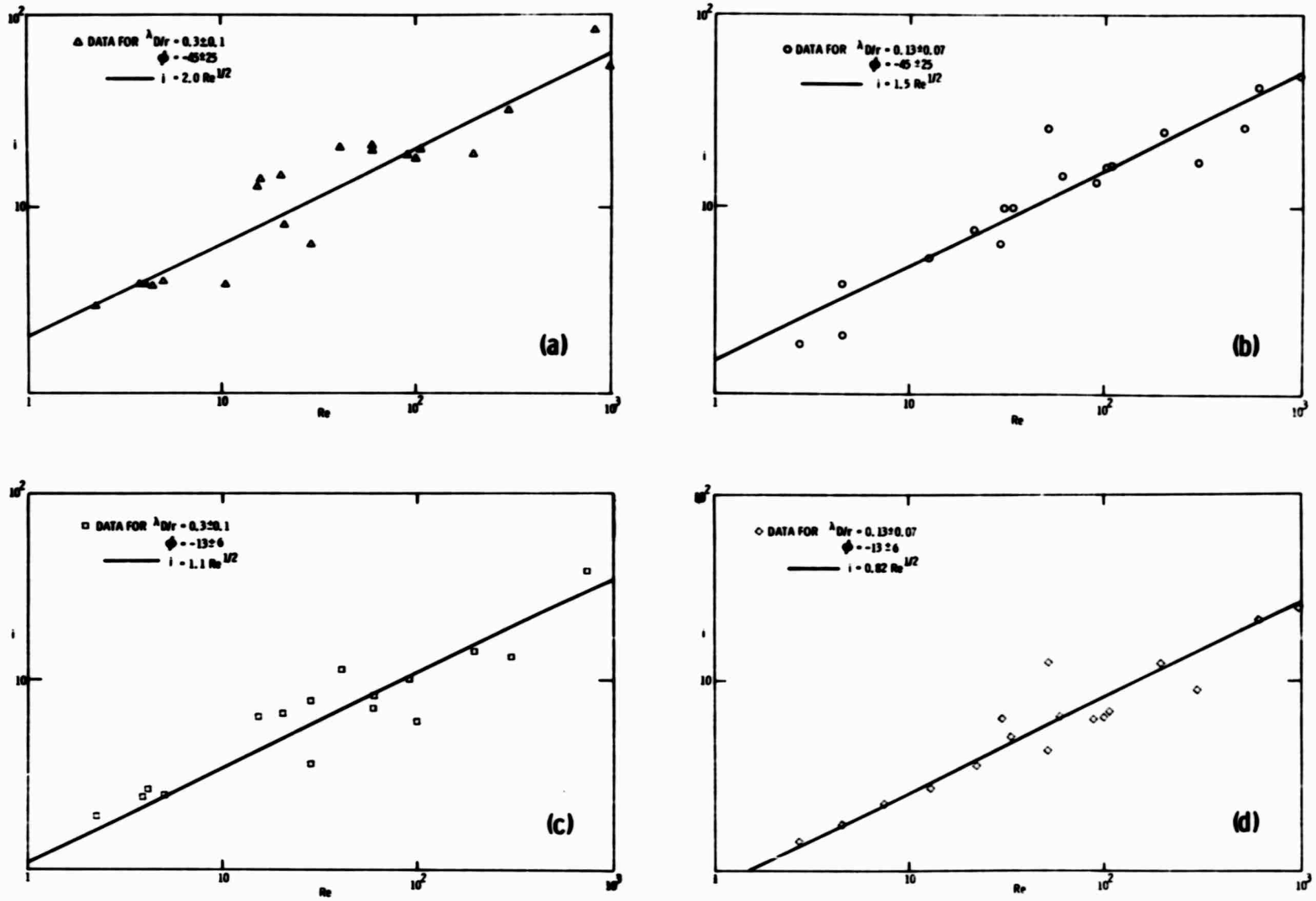

Figure A-3 Calibration of Cylindrical Probe Aligned with Flow (Probe Radius r = 0.11mm, Length ℓ = 20mm, ℓ/r = 182.)

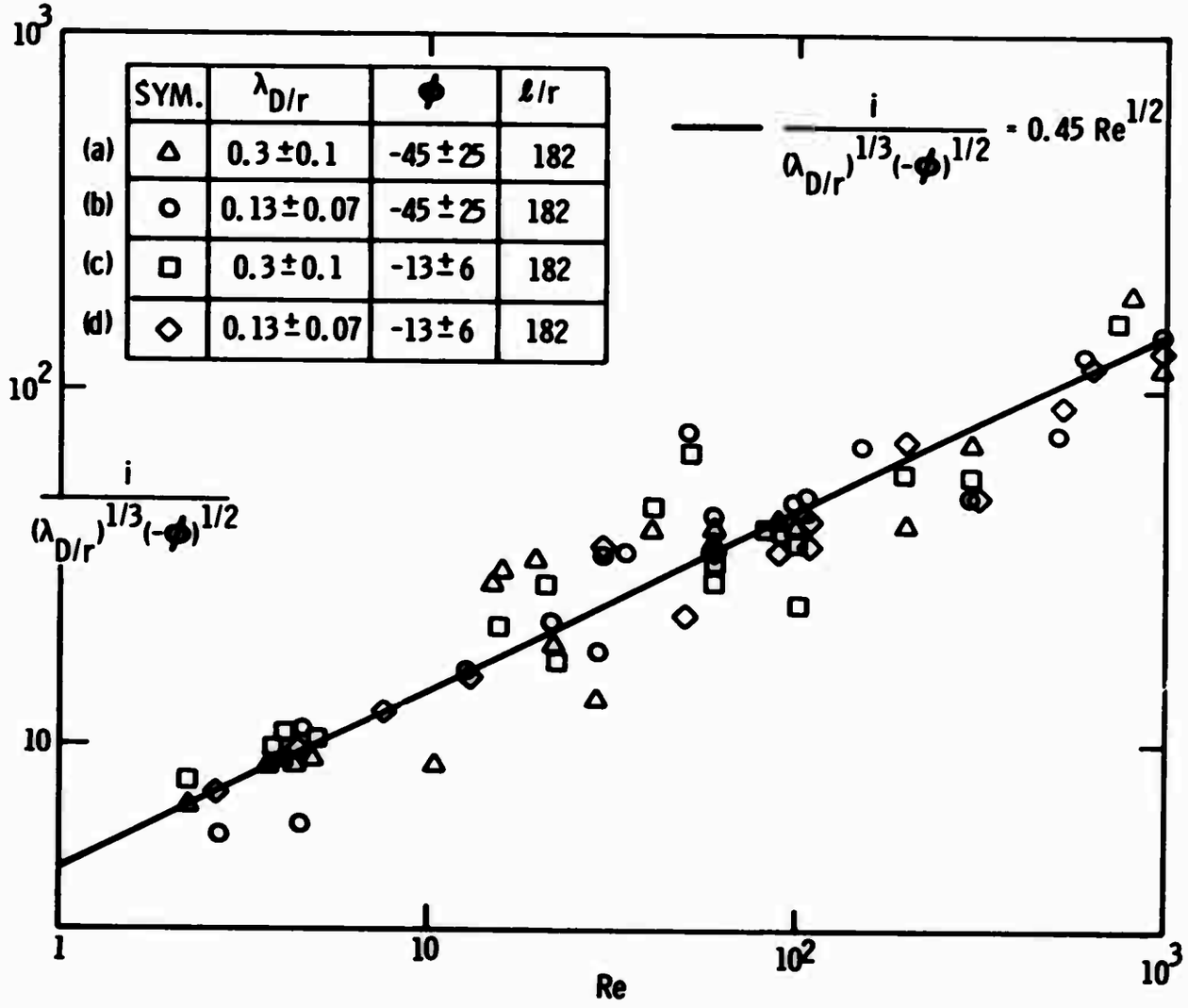

Figure A-4 Correlation of the Data of Figure A-3

APPENDIX B
AN APPROXIMATE THEORY FOR ION COLLECTION BY A CYLINDRICAL PROBE TRANSVERSE TO FLOW

Consider an incompressible, chemically frozen plasma flow over a circular cylinder with its axis perpendicular to the flow velocity. The following ordering is assumed: boundary layer << sheath << probe radius. The method of solution essentially follows that of References 21 and 22. Referring to Figure B-1, we derive the following expression for the ion conservation equation:

$$j(x) = en_{i_\infty} \frac{d}{dx} \left[u(x) \int_0^\infty \left(1 - \frac{n_i}{n_{i_\infty}} \right) \right] dy \qquad \text{(B-1)}$$

where j is the ion current density at x, and u is the flow velocity tangential to the wall. For a cylinder, we use the potential flow solution $u = 2U_\infty \sin\theta$. The above equation can be rewritten in dimensionless form as

$$i(\vartheta) = Sc \cdot Re \cdot \frac{d}{d\vartheta} \left[\sin\theta \cdot \hat{\delta}(\vartheta) \right] \qquad \text{(B-2)}$$

where

$$i = \frac{jr}{en_{i_\infty} D_\infty}$$

is the dimensionless current density (Nusselt number), $Re = \rho_\infty U_\infty 2r/\mu_\infty$ is the Reynolds number, $Sc = \mu_\infty/\rho_\infty D_\infty$ is the Schmidt number based on the ion diffusion coefficient ($Sc \simeq 1$ is assumed in the comparison with experiment), $\theta = x/r$, and

$$\hat{\delta} = \int_0^\infty \left(1 - \frac{n_i}{n_{i_\infty}} \right) d(y/r) \qquad \text{(B-3)}$$

is the dimensionless concentration displacement thickness. Following Reference 3, we construct a one-dimensional, mobility-dominated model for the sheath layer where n_i differs from n_{i_∞}, and, using Poisson's equation and the ion continuity equation and assuming electrons to be absent from the sheath, derive the following expression for δ:

$$\hat{\delta} = \epsilon i \left[\frac{1}{2} + \frac{1}{2} \left(1 + 3 |\phi| / \epsilon i^2 \right)^{2/3} - \left(1 + 3 |\phi| / \epsilon i^2 \right)^{1/3} \right] \qquad \text{(B-4)}$$

where $\epsilon = (\lambda_D/r)^2$ and ϕ is the potential of the body with respect to the undisturbed plasma.

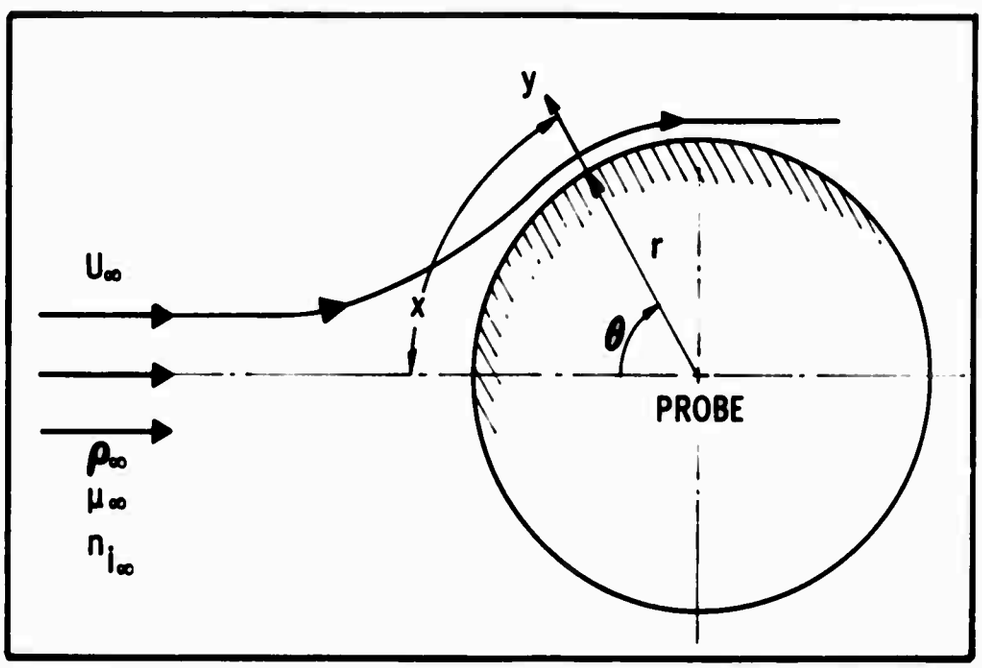

Figure B-1 Coordinates in Probe Theory

Equations (B-1) and (B-4) can be solved for the current distribution $i(\theta)$. For our present purposes, it suffices to consider only the expression for i at the stagnation point, where $\theta = 0$:

$$i_0^2 = \frac{3\,(r/\lambda_D)^2\,|\phi|}{\left[1 + (r/\lambda_D)\,(2/\mathrm{Sc\ Re})^{1/2}\right]^3 - 1} \tag{B-5}$$

Note that for $(\mathrm{Sc\ Re})^{1/2} << r/\lambda_D$, Eq. (B-5) simplifies to

$$i_0 \simeq \left(3\,\frac{\lambda_D}{r}\,|\phi|\right)^{1/2}\left(\frac{\mathrm{Sc\ Re}}{2}\right)^{3/4} \tag{B-6}$$

Finally, we note for purposes of computation that the actual sheath thickness, i.e., the thickness of the layer past which the probe's potential is shielded from the plasma, is given in this formulation by (expressed for the stagnation point):

$$\delta = \lambda_D\,(3/4\,|\phi|)^{1/2}\frac{\left[1 + (r/\lambda_D)\,(2/\mathrm{Sc\ Re})^{1/2}\right]^2 - 1}{\left\{\left[1 + (r/\lambda_D)\,(2/\mathrm{Sc\ Re})^{1/2}\right]^3 - 1\right\}^{1/2}} \tag{B-7}$$

This sheath thickness is shown in Figure A-2 as a function of Re, ϕ and λ_D/r. (The filled circles on the left ordinate are, in descending order, the sheath thickness for Re = 0, calculated from the expressions of Travers and Williams[27] for conditions (a), (b), (c) and (d).) For the sake of comparison, the ratio of boundary layer thickness to probe radius at the stagnation point is also shown in Figure A-2. This quantity is given by $1.6\ Re^{-1/2}$, if the boundary layer thickness[32] is defined as that for which the gas velocity has reached 95% of the inviscid flow value.

Unclassified
Security Classification

DOCUMENT CONTROL DATA - R&D

(Security classification of title, body of abstract and indexing annotation must be entered when the overall report is classified)

1 ORIGINATING ACTIVITY (Corporate author) AC Electronics - Defense Research Laboratories General Motors Corporation Santa Barbara, California	2a REPORT SECURITY CLASSIFICATION Unclassified 2b GROUP -

3 REPORT TITLE

CALIBRATION AND USE OF SPHERICAL AND CYLINDRICAL ELECTROSTATIC PROBES FOR HYPERSONIC WAKE STUDIES

4 DESCRIPTIVE NOTES (Type of report and inclusive dates)

Technical Report

5 AUTHOR(S) (First name, middle initial, last name)

Ian P. French, Richard A. Hayami, Thomas E. Arnold, Martin Steinberg, John P. Appleton, and Arthur A. Sonin

6 REPORT DATE	7a TOTAL NO. OF PAGES	7b NO. OF REFS
May 1970	41	32

8a CONTRACT OR GRANT NO.	9a ORIGINATOR'S REPORT NUMBER(S)
Contract No. F04701-69-C-0125	AC-DRL Report No. TR69-12
b PROJECT NO ARPA Order No. 1341	
c	9b OTHER REPORT NO(S) (Any other numbers that may be assigned this report) SAMSO Report No. TR70-186
d	

10 AVAILABILITY/LIMITATION NOTICES

Distribution of this report is unlimited

11 SUPPLEMENTARY NOTES	12 SPONSORING MILITARY ACTIVITY
	Jointly sponsored by Advanced Research Projects Agency and Space and Missile Systems Organization, Air Force Systems Command.

13 ABSTRACT

An experimental shock tube program was undertaken in order to calibrate electrostatic probes which may be used to make point ion density measurements in continuum flowing plasmas. An empirically derived formula which relates the ion density to the measured probe current was obtained in terms of the appropriate similarity parameters. This empirical correlation was used to interpret the ion currents collected by a radial array of negatively biased spherical probes which were positioned so as to intercept the ionized wake of a hypervelocity model in a ballistics range. The integrated ion densities were found to be in good accord with the integrated electron densities which were simultaneously measured using microwave methods. The application of the electrostatic probe measuring technique to the study of negative-ion chemistry in wakes is also illustrated and briefly discussed.

DD FORM 1 Nov 65 1473 REPLACES DD FORM 1473, 1 JAN 64, WHICH IS OBSOLETE FOR ARMY USE.

Unclassified
Security Classification

14. KEY WORDS	LINK A		LINK B		LINK C	
	ROLE	WT	ROLE	WT	ROLE	WT
Electrostatic probes						
Calibration techniques						
Hypersonic wakes						
Turbulent wakes						
Hypervelocity projectiles						
Shock tubes						
Electron density						
Ion density						
Wake chemistry						
Ballistics ranges						
Microwaves						
Langmuir probes						